Mineralia Slovaca, Web ISSN 1338-3523, ISSN 0369-2086
52, 2 (2020), 103–132, © Authors 2020. CC BY 4.0

Successive formation of Fe and Mn skarns in the Čučma locality (Gemeric unit, W. Carpathians): from metasomatic stage through the amphibolite facies overprint with Ti-rich tephroite to retrograde stilpnomelane-chlorite zone

MARTIN RADVANEC and STANISLAV GONDA

State Geological Institute of Dionýz Štúr, Mlynská dolina 1, SK-817 04 Bratislava, Slovakia

Abstract: Two lenticular ore bodies of Mn bearing skarn, closing a segment of Fe skarn, are located at the northern side of the Čučma village, about 6 km north-east of Rožňava town in the Gemeric unit of the Internal (Inner) Western Carpathians. The Fe and Mn skarns formed during three metamorphic stages. The first stage gradually replaced the former Silurian limestones lenses into of Mn-rich calcite, kutnahorite (kutnohorite – IMA), rhodochrosite, Mn-rich siderite, fluorapatite, tourmaline, phengitic muscovite, Mn-rich chlorite. Rare pyrite, molybdenite, galena, chalcopyrite, pyrite, sphalerite and Ag-rich tetrahedrite occur there as well. Near the contact of former limestone with metapelite, the maghemite dominates over assemblage of Mn-rich carbonates to form Fe skarn. The replacement of limestones as well as the Fe skarn metasomatic origin took place in the chlorite-apatite zone at a temperature range 520–540 °C, where the maghemite and Mn-rich carbonates were generated by the fluid phase, released during anatectic melting of the upper crust during the older Permian metamorphic-magmatic--hydrothermal cycle (MMH of 281–273 Ma).

In the second prograde metamorphic stage, the first-stage minerals were continuously overheated in amphibolite facies (600–650 °C; ~ 4 Kbar), forming following minerals: spessartine, alleghanyite, pyrophanite, manganosite, kempite, jacobsite, iwakiite, hausmannite, tephroite, Ti-rich tephroite, knebelite, rhodonite-1, rhodonite-2, cummingtonite, grunerite and allanite. This study brings an important finding of a new $Ti^{4+} = Si^{4+}$ substitution in the olivine group, where in the Ti-rich tephroite the Si content was replaced by Ti up to 0.159 apfu. Grains formation of Ti tephroite are controlled by the sector zoning, having different content of Ti in each sector.

In the final stage of skarns formation, the unstable minerals of previous two stages were replaced by the Si, Ba, H_2S and H_2O bearing fluid phase to form Ca-rich spessartine, bementite, pyrochroite, quartz, pyrolusite, baryte, chlorite and stilpnomelane during the retrograde stilpnomelane-chlorite zone metamorphism at 300–370 °C. This mineral assemblage was gradually formed in retrograde metamorphic path with decreasing temperature from the amphibolite facies to the stilpnomelane-chlorite zone. The prograde and retrograde metamorphic stages produced a group of Mn bearing garnets, humites, oxides, halides, spinels, olivines, pyroxenoides, amphiboles and they on the former Fe skarn formed a younger and fine to medium-grained Mn bearing part of the skarn. This metamorphic part of Mn skarn has the positive Eu anomaly and was formed by the fluid phase influenced by the primitive mantle in younger MMH cycle of the Permian, dated to 269–251 Ma.

In the paper, altogether 39 empiric reactions describe the successive formation of skarns. The source of Fe, Mn and Ba, necessary to skarns formation, was released to fluid phase by anatectic melting of the Silurian rhyolite and Devonian stratabound sulfidic mineralization in the Permian amphibolite facies metamorphism.

Key words: Fe skarn, Mn skarn, maghemite, rhodochrosite, manganosite, kempite, rhodonite, Mn-rich spinels, Ti-rich tephroite, Pernian MMH cycle, Gemeric unit

Graphical abstract

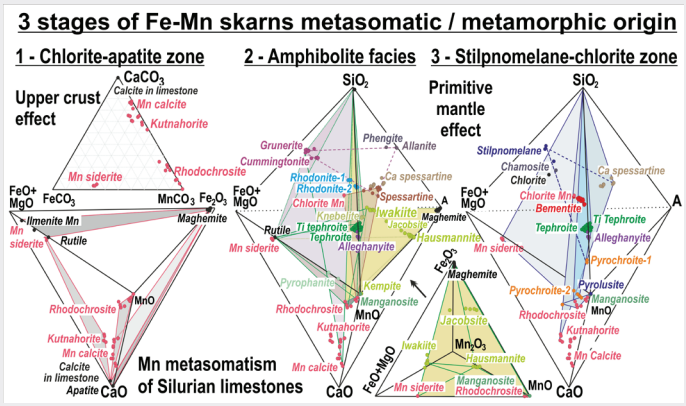

Highlights

Three successive steps of Fe and Mn skarns formation were revealed:

1. Metasomatic stage in chlorite-apatite zone with rhodochrosite, kutnahorite and maghemite.
2. Metamorphic overprint in amphibolite facies with Ti-rich tephroite, Mn-olivines, spinels, rhodonite, manganosite and amphiboles.
3. Retrograde stilpnomelane-chlorite zone.

Introduction

Two lenticular ore bodies of Mn bearing skarn closing a segment of Fe skarn, known as the Black Mine (Feketebánya) or the Roszty Mine, are located at the northern side of the Čučma village on the western slope of the Stredná hill, about 6 km north-east of Rožňava town in the Gemeric unit (Fig. 1). The Gemeric unit is a part of the Internal (Inner) Western Carpathians. The Mn skarn was mined from the second half of the 19th century until the beginning of the 20th century. The subject of mining was mainly its part bearing pyrolusite (Bartalský et al., 1973; Grecula et al., 1995). The length of skarns bodies is 50 to 100 m, thickness 1–4 m, direction VSV and dip 50–60° to the south, having tectonic contact with the surrounding sericite-graphite phyllites (Bartalský et al., 1973; Grecula et al., 1995). The formation of Fe-Mn skarns is genetically dependent on occurrence of host limestones, being a host rock of Fe-Mn mineralization (Kantor, 1953; Grecula et al., 1995). In the Čučma area, altogether eight crystalline limestone lenses occur in serite-graphite phyllites, graphite phyllites and lydite beds of Betliar Fm of Silurian age. The limestone lenses of EW direction and length up to 300 m are white, consisting of metamorphosed calcite. Their thickness is less than 5 m and dip 50–60° to the south (Fig. 1; Kantor, 1953; Grecula et al., 2009). In crystalline limestones the diopside and grossular with an andradite molecule content of up to 21 mol% were locally found (Ružička et al., 2020). Elsewhere the Mn rich garnet, muscovite, chlorite, pyrite, quarz and amphibole occur in lenses respectively. The amphibole there has a prismatic shape and, according to its optical properties Kantor (1953) considered it as a tremolite. Near the transition zone to Mn mineralization in limestone lenses the short veins of Mn-rich calcite and pyrrhotite were found, though the amphibole has also been found in rocks around the limestone lenses (Kantor, 1953).

The body of Mn skarn in the former limestone reaches a thickness of 1.3 to 4 m and its length is 50–100 m. According to the mining maps from 1940 the Mn skarn does not exceed a depth of 15–20 m. The available field data provide an information on two separate skarn lenses in host limestones and information about their genesis indicates that conversion of limestone to skarn was at the beginning selectively metasomatic and later metamorphic, related to Variscan metamorphism (Kantor, 1953; Rojkovič, 1999, 2001).

In previous studies various authors focused on the description of the main Mn bearing mineralization, although the occurrence of Fe-rich oxides in the skarn was not negligible. These mineralogical studies confirmed that the main Mn-bearing mineralization of the skarn consists of rhodonite, rhodochrosite, kutnahorite (kutnohorite – IMA), pyroxmangite, spessartine, tephroite, calcite, Mn-rich calcite, quartz, hematite and Mn-rich magnetite. Rarely there occurred baryte, bementite, caryopilite, fluorapatite, hübnerite, pyrophanite, hausmannite, mangano-

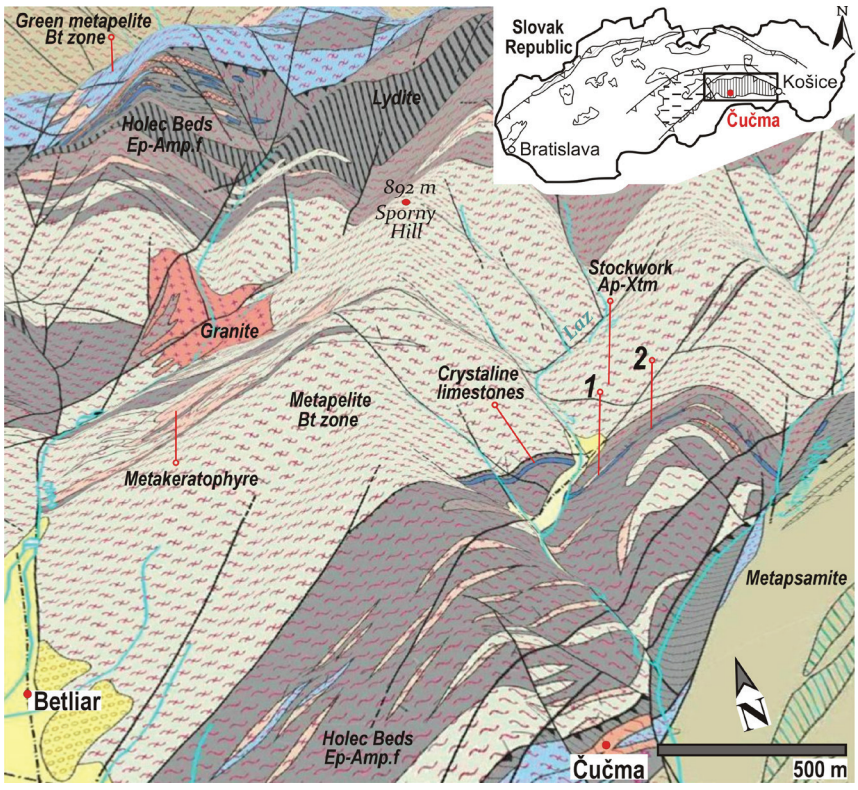

Fig. 1. Geological map and metamorphic zonality of Čučma area in the 3D model according to Grecula et al. (2009). **1** – Mn bearing skarn and **2** – Fe and Mn bearing skarn positions in crystalline limestone. The Holec Beds – a part the Silurian Betliar Fm are built of crystalline limestone, sericite-graphite phyllites, graphite phyllites and lydite. The position of apatite-xenotime stockwork is explained in more details in Radvanec & Gonda (2019).

site, jacobsite, pyrosmalite-(Mn), rutile, stilpnomelane, muscovite, biotite, chlorite, albite, allanite-(Ce), quartz and prismatic amphiboles regarded as anthophyllite and tremolite. Disseminated sulfides such as alabandite, arsenopyrite, bismuthinite, galena, gersdorffite, glaucodote, chalcopyrite, cobaltite, pentlandite, pyrite, pyrrhotite, sphalerite and ullmannite were also locally found. The goethite, limonite, cryptomelane, manganite, melanterite, pyrolusite, sulfur, chamosite and todorokite occur in the supergenic mineralization zone (Kantor, 1953, 1954; Bartalský et al., 1973; Faryad, 1994; Grecula et al., 1995; Rojkovič, 2001; Peterec & Ďuďa, 2003; Peterec & Ďuďa, 2009; Števko et al., 2015). However, in published analyses of pyroxenoides (rhodonite, pyroxmangite) the content of $CaSiO_3$ ranges from 7.8 to 8.8 mol.% and according to the Momoi (1964) classification, the $CaSiO_3$ content clearly shows generations of Fe-rich and pure rhodonite, so the published analyses of pyroxenoides by Rojkovič (2001) stated that pyroxmangite is the rhodonite as well.

The aim of present mineralogical and petrological study is to supplement by new data to previous findings about the development of skarns in the Čučma area (Fig. 1). In addition to the abovementioned minerals, we have identified following minerals: Ti-rich tephroite, knebelite, maghemite, spinels from the iwakiite-jacobsite to hausmannite series, kempite, alleghanyite, pyrochroite, rhodonite, cummingtonite, grunerite, tourmaline, molybdenite and Ag-rich tetrahedrite. An important finding of this study is showing a new substitution in the olivine group, where the Si content is replaced by Ti up to 0.159 apfu in the Ti-rich tephroite. All new findings helped to identify the empirical reactions explaining the successive formation of the skarn from the stage when Mn carbonates and the Fe bearing part entered to the final stage of the Mn bearing skarn formation, depending on change of metasomatic and metamorphic conditions. The results on the formation of Mn mineralization complement the genetic model of Permian hydrothermal mineralization in the Gemeric unit, which was presented by Radvanec & Gonda (2019).

Geological setting

Skarn represents mostly fine to medium-grained dark rock with a reddish-brown tint. Sometimes it is black or it has a pink colour respectively. Texture of skarn is most often fibro-granoblastic, less often granoblastic massively smoky or frequently banded (Figs. 2, 3, 4, 6, 7 and 9). Two bodies of skarn are tectonically separated and they are a part of the Holec Beds of Betliar Fm encompassing the Early Paleozoic – Silurian evolution of Gemeric unit (Grecula et al., 2009). The Holec Beds consist of sericite-graphite phyllites, lenses of lydite and crystalline limestones bearing skarn in the Čučma area (Fig. 1). This occurrence of Holec Beds was metamorphosed in epidote-amphibolite facies and a part of former limestone lenses was replaced by minerals of skarn (Kantor, 1953; Grecula et al., 2009; see Fig. 1 in Radvanec & Gonda, 2019). In the same position, on the lenses of former Silurian limestones, the Fe bearing skarn was formed in localities of Dlhá dolina area, Lipový and Hekerová hills (Radvanec & Gonda, 2019; Kantor, 1954). The Fe bearing skarn from Dlhá dolina was formed in the stilpnomelane-chlorite zone of Permian metamorphic-magmatic-hydrothermal cycle (MMH cycle). This skarn was found in the direct contact with the limestone lens as well as the direct contact with the magnesite body (Radvanec & Gonda, 2019). Position of skarn from Dlhá dolina area, Lipový and Hekerová hills is comparable with that of the Čučma skarn, however the development of the skarn in Čučma locality was gradual. Firstly a part of Fe skarn was formed and later there dominated Mn-type skarn (Figs. 3 and 4).

Methodology

Mineralogical, geochemical and petrological research was applied on two skarn bodies in known localities of Čučma area (Fig. 1).

The skarn mineralization was studied in samples from two dumps (dump-1; 48° 42‘ 31.05“ N, 20° 32‘ 55.53“ E; dump-2 (48° 42‘ 37.34“ N, 20° 33‘ 14.95“ E), applying polished thin sections and EMPA analyses. All above listed type rocks and mineralizations were analysed by quantitative analyses (Tab. 5). Chemical analyses were done in SGIDŠ GAL Laboratories in Spišská Nová Ves, Slovakia. The EMPA mineral analyses and their crystallization succession were obtained in the SGIDŠ Department of microanalysis, Bratislava. The Cameca SX-100 electron microscope was equipped by three spectrometers and Kevex delta IV EDS system. The natural and synthetic standards were used for calibration. Measuring conditions: acceleration voltages 15 KV and 25 KV, current 10 nA at analyses of carbonates or 20 nA at silicate analyses. The diameter of the electron beam was changed according to the type and size of minerals. Stilpnomelane and Mn-rich micas were measured by widened beam 7–10 μm, carbonates 10–15 μm and other minerals by 2–5 μm beam. The measurement time from 10 to 35 s was chosen with regard to achieve the required measurement accuracy of given element. Detection limit for individual elements is smaller than 0.05 wt.% with an error 1-sigma.

New mineralogical data in above listed places were classified in the same way. After study by optical microscope the EMPA results for all revealed minerals were projected in triangles and tetrahedrons, regarding three successive stages of skarn formations. These projections were done for carbonates, spinels, oxides, silicates and others minerals. Carbonates were projected in triangle diagrams of $FeCO_3$ – $MnCO_3$ – $CaCO_3$ resp. with end-members siderite, rhodochrosite and calcite

(Fig. 5). The projection of all analyses after re-calculation to chemical formula were shown in tetrahedron projections: FeO+MgO – CaO – Fe_2O_3 – MnO, FeO+MgO – MnO – A – SiO_2 and FeO+MgO – MnO – Fe_2O_3 – Mn_2O_3. In stages 2 and 3 of skarn formation, mineral position was visualized in individual tetrahedron projections, but their final processing were joined into one entity (Fig. 10). These projections intended their exact view in successive crystallization system of skarn, which is the result of 39 reactions. In projections the indexed minerals are shown, classifying individual mineralizations to zones from the chlorite-apatite zone through amphibolite facies to final stilpnomelane-chlorite zone.

The chemical analyses of Early Paleozoic metarhyolite from the outcrop on Stromíš hill (48° 48‘ 23.89“ N, 20° 27‘ 0.82“ E) and of S-type Permian granites from localities of medium- to fine-grained muscovite bearing granite from Dlhá dolina-Elisabeth mine (48° 46‘ 18.72“ N, 20° 32‘ 36.38“ E), the medium grained muscovite-biotite granite from the Súľová locality (48° 48‘ 57.31“ N, 20° 28‘ 29.59“ E) and three samples of skarn from Čučma area are shown in Table 5. The sample of Early Paleozoic metarhyolite supplemented previously published data on Early Paleozoic stratabound sulfidic mineralization of Smolník type and lydites as a source of elements in hydrothermal mineralization, which was formed in Permian after melting of these rocks in amphibolite facies. This anatectic melting, producing S-type granites in Permian, also released elements from Early Paleozoic rocks into the fluid phase. Various mineral associations crystallized from this fluid phase depending on temperature and pressure decrease from the anatectic zone toward the surface (Radvanec & Gonda, 2019). The collection of S-type granite analyses was supplemented by two samples from localities of Dlhá dolina and Súľová (Tab. 5). All these granites formed in hotlines above subduction zone during the Permian development of Paleo-Gemericum during the metamorphic-magmatic-hydrothermal (MMH) cycle of Radvanec et al. (2009) and Radvanec & Gonda (2019).

Three bulk chemical analyses of skarn, Lower Paleozoic metarhyolite and S-type granites (Dlhá dolina and Súľová occurrences) were normalized according to REE standards (Sun and McDonough, 1989). Two distinguished groups of investigated samples suit to genetic model of Permian hydrothermal mineralization in Gemeric unit (Radvanec & Gonda, 2019): Older group suits to upper crust normalization and the second, younger group of samples suits to primitive mantle normalization (Fig. 11). Applying this REE normalization, the skarn samples were divided into “upper crust” and “primitive mantle” groups. Both groups are fully in line with their geotectonic background and formation of two age-different groups of anatectic S-type granite. Because S-type granites represent product of anatexis in amphibolite facies, in subsequent processing the group of analyses of the “upper crust” was normalized on porphyric granite, representing the source non-differentiated anatectic melt. This anatectic melt generated fluid phase, from

Tab. 1
Representative analyses of carbonates in Čučma skarns.

Mineral	Mn calcite	Kutnahorite	Kutnahorite	Kutnahorite	Mn siderite	Rhodochrosite	Rhodochrosite	Rhodochrosite	Rhodochrosite	Calcite
Place	matrix	matrix	matrix	matrix	in MnCal	matrix	matrix	matrix	matrix	Relict
Stage	1	1	1	1	1	1	1	1	1	Limestone
Process	Metasomatic	Metasomatic	Metasomatic	Metasomatic	Metasomatic	Metasomatic	Metasomatic	Metasomatic	Metasomatic	Silurian
FeO	0.36	0.67	1.81	6.07	39.64	1.18	3.32	0.97	0.18	0.14
MnO	14.39	29.59	25.37	16.15	16.73	46.97	47.48	49.89	61.03	0.27
MgO	0.19	0.74	0.98	1.22	2.70	1.06	0.90	0.60	0.07	0.71
CaO	42.31	27.83	30.14	34.46	1.93	10.94	8.51	8.79	0.32	55.52
CO_2	42.56	41.41	41.57	42.13	39.10	39.61	39.17	39.08	38.32	44.63
Total	99.81	100.23	99.87	100.02	100.10	99.77	99.38	99.33	99.93	101.28
Fe	0.005	0.01	0.027	0.088	0.621	0.018	0.052	0.015	0.003	0.002
Mn	0.21	0.443	0.379	0.238	0.265	0.736	0.752	0.792	0.988	0.004
Mg	0.005	0.019	0.026	0.032	0.075	0.029	0.025	0.017	0.002	0.018
Ca	0.78	0.527	0.569	0.642	0.039	0.217	0.171	0.177	0.007	0.976
$CaCO_3$	78.00	52.75	56.84	64.20	3.90	21.70	17.10	17.68	0.70	97.60
$MgCO_3$	0.50	1.90	2.60	3.20	7.50	2.90	2.50	1.70	0.20	1.80
$FeCO_3$	0.50	1.00	2.70	8.80	62.10	1.80	5.20	1.50	0.30	0.20
$MnCO_3$	21.00	44.34	37.86	23.80	26.50	73.60	75.20	79.12	98.80	0.40

which mineralization with the upper crust characteristics originated in the granite exocontact. According to REE normalization this mineralization complies with the source porphyric granite. Variation of elements contents from the group of "upper crust" after normalization to porphyric granite was visualized in isocones (isoconcentrations) and in the logarithmic scale they were evaluated as enrichment or deficiency in the element content. After normalization of element content to granites, the isocone in compared sample is the same in the case of their ratio equal to 1. In good agreement with the reference granite an isocone falls within the range 0.1–10. Values beneath 0.1 represent a deficiency and above 10 the enrichment against granites (Figs. 12–14). The contents of elements have colour division and division to groups, respecting the results of mineralogical investigation and binding of elements in mineral associations, found in type localities by mineralogical and geochemical investigation. Part of the main components of analyses and unclassified element contents occur in the black group. The red and green groups belong to elements prevailingly from apophyses, greisens and stockworks. Yellow group is formed by elements from the stockwork mineralization and blue group belongs to elements of vein mineral association (Fig. 13; Radvanec & Gonda, 2019).

The second – younger group of Permian hydrothermal mineralization, having the influence of primitive mantle, was normalized on younger differentiated granite, which correspondingly was displayed as enrichment or deficiency of the element content respectively (Fig. 14).

Minerals in successive formation of skarn

First Mn metasomatic stage and Fe bearing skarn formation

The first Mn metasomatic stage gradually replaced the former Silurian limestones lenses into of Mn-rich calcite, kutnahorite, rhodochrosite, Mn-rich siderite, fluorapatite, tourmaline, phengitic muscovite, Mn-rich chlorite and pyrite. Isolated grains of molybdenite, galena, chalcopyrite, pyrite, sphalerite and Ag-rich tetrahedrite here in the matrix of Mn-rich calcite and kutnahorite were also found (Figs. 2, 3b and 9.). Relics of Mn-rich chlorite, which reach a size of up to 50 μm, have been rarely found together with rhodochrosite (Fig. 7e). However the unreacted relics of former calcite (limestone), Mn chlorite are still frequently present, usually in spessartine and in the grossular/spessartine matrix (Fig. 2). The MnO content in Mn chlorite ranges from 4.45 to 24.71 wt.% and its chemical formula is variable, from the Mn-rich clinochlore to the end member of pennantite (Tab. 2).

The main minerals of this metasomatic stage are Mn calcite, kutnahorite and rhodochrosite (Tab. 1). Between the end members of kutnahorite and rhodochrosite, a group of Mn carbonates was found where the content of $MnCO_3$ (6 analyses) ranges from 60.5 to 78.3 mol. % (Fig. 10a). According to the Mn carbonate thermometer in the $CaCO_3$–$MnCO_3$ system, this range of the $MnCO_3$ content shows the formation of rhodochrosite and kutnahorite at the temperature from 520° to 540 °C (De Capitani & Peters, 1981; Chang et al., 1998).

In the direct contact of former limestone lens at the metapelite, a Fe bearing skarn originated during the metasomatic first stage, and it reaches here a thickness of about 6 cm. The Fe skarn is of black colour having pseudo cast monomineral form of **maghemite** (Fe_2O_3) and therefore the Fe skarn is weakly magnetic. The mass of zonal maghemite with size up to 50 μm, fluorapatite up to 40 μm, rutile, ilmenite where the Mn content reaches up to 7.74 wt.% and aggregates of pyrite up to 150 μm in size are the maim assemblage of the Fe skarn. In the pyrite, the inclusions of chalcopyrite and galena are frequently present and the rim of pyrite contains a variable As content up to 5 wt.% (Fig. 3).

Fluorapatite belongs to one of first minerals formed during the replacement of former limestone. It forms inclusions in kutnahorite, relics in spessartine and as well as together with kutnahorite it is enclosed in the mass of maghemite respectively (Fig. 2a, 3c, 7c and 9b–c). The homogeneous grains of fluorapatite do not contain any admixture of other elements and its chemical formula is close to end-member $Ca_5(PO_4)_3F$ (Tab. 2). In different localities of Gemeric unit the same pure fluorapatite in assemblage with tourmaline, biotite, phengitic muscovite, margarite, topaz, stilpnomelane, chlorite, quartz, fluorite, calcite, cassiterite, ankerite, dolomite, kutnahorite, rhodochrosite, siderite, magnesite, allanite, goyazite, In-rich sulfides and U-rich minerals occur. In all these localities from greisens in the depth and direct contact with granite to U-SedEx mineralization on the surface, the fluorapatite does not contain any admixture of other elements, however it was formed in different P-T conditions of the Permian hydrothermal mineralization in Gemeric unit (Radvanec & Gonda, 2019). The zone, where the fluorapatite occurs with phengitic muscovite and chlorite, was named the chlorite-apatite zone and this zone has a regional enlargement in the Permian hydrothermal mineralization (l. c.). The origin of studied fluorapatite is conditioned by the existence of calcite or limestone, which reacted with residual Fe-bearing fluid phase with H_3PO_4 content forming fluorapatite and maghemite according to reaction (1). Reaction 1 runs simultaneously with Mn metasomatism of limestone to form Mn calcite, kutnahorite and rhodochrosite respectively.

The matrix of Fe skarn is dominantly formed by aggregates of zonal maghemite. In the maghemite core the content of SiO_2 always ranges from 1.12 to 4.77 wt.%, however its rim is almost free of SiO_2 and sometimes contains only 0.08 wt.% of SiO_2 (Fig. 3). According to

Tab. 2
Representative analyses of minerals in Čučma skarns.

Mineral	Fluorapatite	Alleghanyite	Ca spessartine	Ca spessartine	Ca spessartine	Spessartine	Pennantite	Kempite	Grunerite	Cummingtonite	Chlorite	Stilpnomelane	Stilpnomelane	Pyrochroite-1	Pyrochroite-2
Place	in Fe-Mn skarns	in oxides	rim Fe skarn	rim Fe skarn	rim Fe skarn	rim Fe skarn	matrix	rim MnO	matrix	matrix	matrix	in Mn skarn	in Fe skarn	in tephroite	in Mn carbonate
Stage	1	2	2	2	2	2	2	2	2	2	3	3	3	3	3
Process	Metasomatic	Prog.-metam.	Prog.-metam.	Prog.-metam.	Prog.-metam.	Prog.-metam.	Prog.-metam.	Prog.-metam.	Prog.-metam.	Prog.-metam.	Retro.-metam	Retro.-metam	Retro.-metam	Retro.-metam	Retro.-metam
SiO_2	0.02	23.19	35.81	36.06	37.18	35.52	26.25	0.09	51.46	53.17	46.25	44.93	44.07	5.31	0.09
TiO_2	0.00	0.01	0.15	0.13	0.09	0.03	0.01	0.00	0.00	0.00	0.00	0.01	0.01	0.00	0.00
Al_2O_3	0.00	0.00	18.71	18.82	20.21	20.21	17.37	0.00	0.01	0.10	5.30	2.86	5.56	0.00	0.00
Cr_2O_3	0.00	0.00	0.00	0.00	0.02	0.02	0.02	0.00	0.00	0.00	0.00	0.00	0.00	0.00	0.00
FeO	1.79	0.16	3.52	0.00	1.41	0.00	9.43	0.22	32.51	24.34	30.89	0.00	0.00	2.10	0.95
Fe_2O_3	0.00	0.00	4.54	5.19	2.40	0.99	0.00	0.00	0.00	0.00	0.00	28.52	35.50	0.00	0.00
MnO	0.2	72.42	31.45	29.12	24.35	41.42	24.71	73.12	6.06	7.74	0.43	15.21	1.02	70.05	70.52
MgO	0.03	0.24	0.07	0.06	0.01	0.03	11.37	0.02	7.57	12.29	4.47	3.06	4.53	0.06	1.28
CaO	54.66	0.06	5.83	10.74	14.38	1.87	0.03	0.12	0.48	1.18	0.52	0.05	0.58	0.25	6.13
Na_2O	0.01	0.00	0.00	0.00	0.00	0.00	0.00	0.03	0.00	0.02	0.04	0.07	0.13	0.14	0.00
K_2O	0.01	0.00	0.00	0.00	0.00	0.00	0.00	0.02	0.00	0.00	0.84	1.84	2.26	0.02	0.00
P_2O_5	41.26	0.00	0.00	0.00	0.00	0.00	0.00	0.00	0.00	0.00	0.00	0.00	0.00	0.00	0.00
F	4.38	0.00	0.00	0.00	0.00	0.00	0.00	0.16	0.00	0.00	0.00	0.00	0.00	0.00	0.00
Cl	0.00	0.00	0.00	0.00	0.00	0.00	0.01	15.45	0.00	0.01	0.00	0.05	0.01	0.00	0.00
H_2O	0.00	3.61	0.00	0.00	0.00	0.00	11.05	14.74	0.00	0.00	11.64	2.22	1.26	21.65	20.74
Total	102.35	99.69	100.07	100.11	100.05	100.08	100.25	103.97	98.09	98.85	100.38	98.82	94.93	99.58	99.70
OFCl	1.84							3.55							
OF	0.00							0.07							
OCl	0.00							3.49							
$Total_C$	100.51							100.42							
Si	0.002	1.927	2.944	2.930	2.970	2.938	5.695	0.003	8.048	7.990	4.766	10.550	10.432	0.073	0.001
Al^{IV}	0.000	0.000	0.056	0.070	0.030	0.062	2.305	0.000	0.000	0.010	0.234	0.000	0.000	0.000	0.000
Sum_{-T}	0.000	1.927	0.000	0.000	0.000	0.000	8.000	0.003	0.000	0.000	5.000	10.550	10.432	0.073	0.001
Al^{VI}	0.000	0.000	1.757	1.732	1.873	1.908	2.133	0.000	0.002	0.007	0.409	0.791	1.550	0.000	0.000
Ti	0.000	0.001	0.009	0.008	0.006	0.002	0.002	0.000	0.000	0.000	0.000	0.002	0.002	0.000	0.000
Fe^{3+}	0.000	0.000	0.281	0.317	0.144	0.062	0.000	0.000	0.000	0.009	0.000	5.034	6.317	0.000	0.000
Fe^{2+}	0.127	0.011	0.242	0.000	0.094	0.000	1.711	0.006	4.252	3.050	2.662	0.000	0.000	0.024	0.011
Cr	0.000	0.000	0.000	0.000	0.001	0.001	0.003	0.000	0.000	0.000	0.000	0.000	0.000	0.000	0.000
Mn	0.014	5.098	2.190	2.004	1.648	2.902	4.541	1.982	0.803	0.985	0.038	3.025	0.205	0.822	0.863
Mg	0.004	0.030	0.008	0.008	0.002	0.003	3.678	0.001	1.765	2.753	0.687	1.071	1.599	0.001	0.028
Ca	4.958	0.005	0.513	0.935	1.231	0.165	0.007	0.004	0.080	0.190	0.057	0.013	0.147	0.004	0.095
Na	0.002	0.000	0.000	0.000	0.000	0.000	0.000	0.002	0.000	0.006	0.008	0.032	0.060	0.004	0.000
K	0.000	0.000	0.000	0.000	0.000	0.000	0.000	0.001	0.000	0.000	0.110	0.551	0.682	0.000	0.000
P	2.957		0.000	0.000	0.000	0.000	0.000	0.000	0.000	0.000	0.000	0.000	0.000	0.000	0.000
Cations	8.064	7.072	8.000	8.003	8.000	8.044	20.075	1.999	14.950	15.000	8.971	21.069	20.994	0.928	0.998
CF	2.345	0.000	0.000	0.000	0.000	0.000	0.000	0.032	0.000	0.003	0.000	0.000	0.000	0.000	0.000
CCl	0.000	0.000	0.000	0.000	0.000	0.000	0.007	1.677	0.000	0.000	0.000	0.040	0.008	0.000	0.000
OH	1	2.00	0.00	0.00	0.00	0.00	16.00	3.15	0.00	0.00	0.00	3.48	2.00	2.00	2.00
O	13	10	12	12	12	12	36	4	23	23	18	36	36	2	2

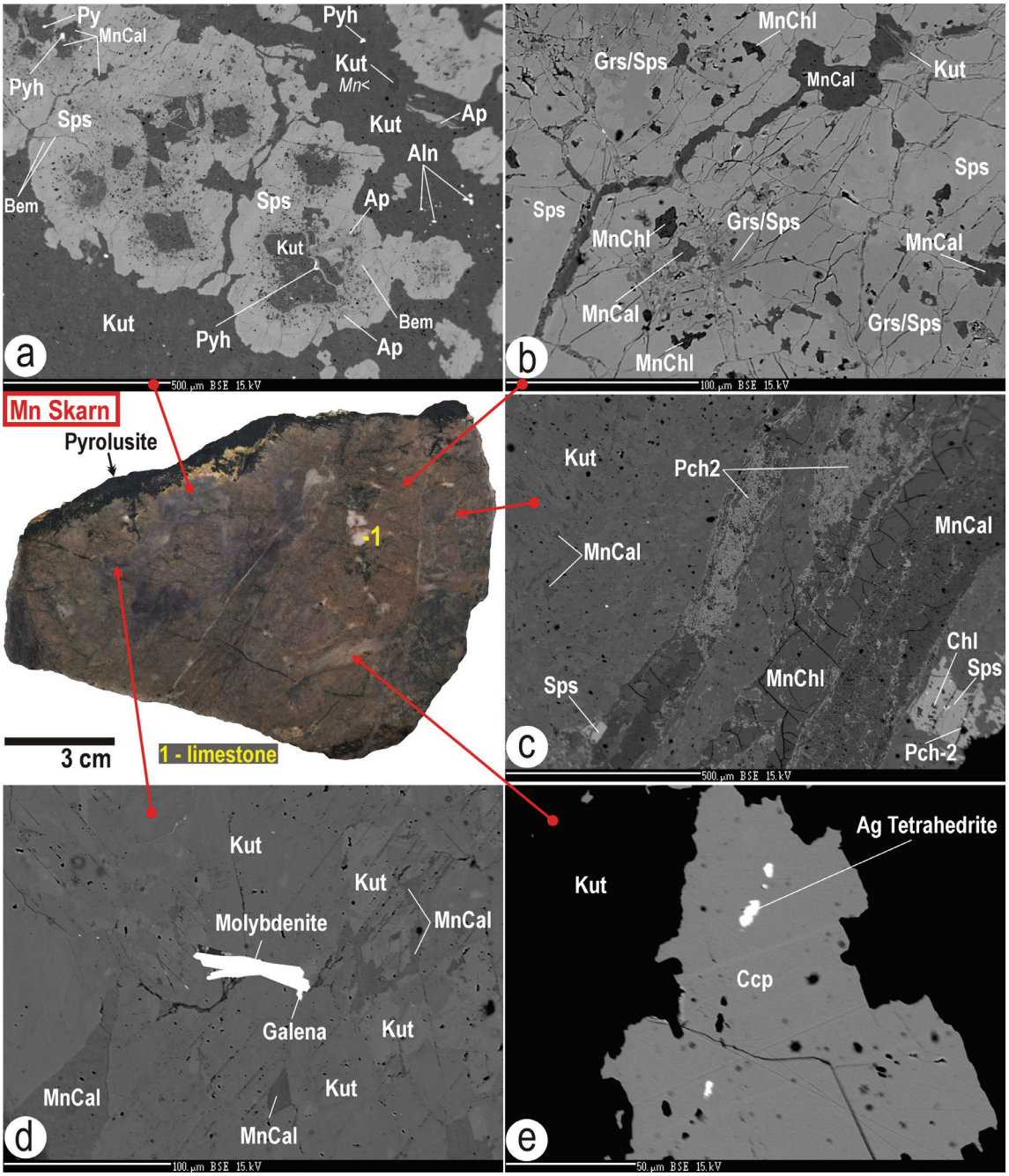

Fig. 2. Metasomatic onset of the Mn skarn formation shows by kutnahorite (Kut) and Mn-rich calcite areas (see cross-section) and other spots in the BSE images. **a** – The spot where kutnahorite and Mn calcite were replaced by spessartine (Sps) of atoll shapes. This garnet formed in second metamorphic stage of Mn skarn formation; pyrite (Py), pyrophanite (Pyh), bementite (Bem), fluorapatite (Ap), allanite (Aln). **b** – Place of spessartine with spots of Ca-rich spessartine (Grs/Sps) and relics of Mn calcite and Mn-rich chlorite (MnChl). **c** – Place of kutnahorite with spessartine, Mn chlorite and veined pyrochroite-2 (Pch-2), chlorite (Chl) in spessartine. **d** – Place with disseminated molybdenite and galena in matrix of kutnahorite and Mn calcite. **e** – This place shows disseminated chalcopyrite (Ccp) with inclusions of Ag-rich tetrahedrite in kutnahorite matrix.

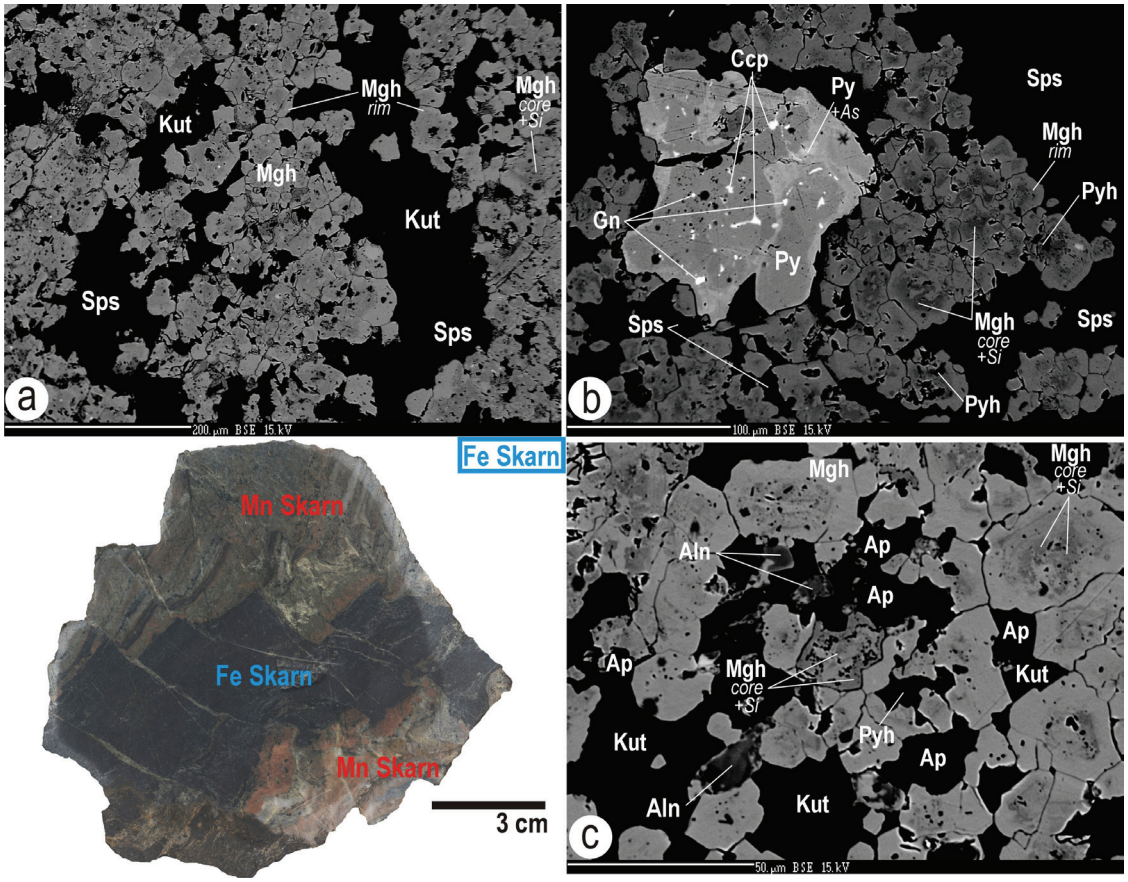

Fig. 3. Successive formation of skarn in the contact of former limestone lens (cross-section) and metapelite. The black Fe bearing part of skarn represents its formation during the first metasomatic stage, than the Fe skarn was rimed by Mn bearing skarn formed in second metamorphic stage. The BSE images show mineral assemblages in the part of Fe skarn. **a** – In aggregates the cores of individual maghemite (Mgh) contains Si and their rims are of pure maghemite. The space in maghemite aggregates is filed by kutnahorite (Kut) and by spessartine (Sps). **b**, **c** – Si-rich core and pure rim of maghemite. Disseminated pyrite (Py) with inclusions of galena (Gn), chalcopyrite (Ccp) and zones rich of As in pyrite. Position of fluorapatite (Ap), allanite (Aln), pyrophanite (Pyh), kutnahorite, and spessartine in maghemite aggregates.

unclear chemical formulas based on EMPA, there is a risk that the SiO_2 content is bound in the submicroscopic form of quartz to the core of maghemite and therefore the determined SiO_2 content does not belong to the real formula of maghemite. In each grain of zonal maghemite, the F content is always present in the range from 0.28 to 0.37 % wt.% (Tab. 3).

According to identified minerals and their relationships in the metasomatic replaced limestones and minerals in the Fe skarn, following six reactions were inferred.

$$5CaCO_3 + 2Fe^{3+}O(OH) + 3H_3PO_4 + HF = Fe_2O_3 + Ca_5(PO_4)_3F + 6H_2O + 5CO_2 \quad (1)$$
Limestone — Fe/P-bearing fluid phase — Maghemite — Apatite

$$CaCO_3 + 2FeO(OH) + Mn(OH)_2 + CO_2 = Fe_2O_3 + CaMn(CO_3)_2 + 2H_2O \quad (2)$$
Limestone — Fe/Mn-bearing fluid phase — Maghemite — Kutnahorite

$$CaCO_3 + Fe(OH)_2 + Mn(OH)_2 + 2CO_2 = FeCO_3 + CaMn(CO_3)_2 + 2H_2O \quad (3)$$
Limestone — Fe/Mn-bearing fluid phase — Siderite — Kutnahorite

$$Fe_2O_3 + 2TiO_2 = 2FeTiO_3 + 0.5O_2 \quad (4)$$
Maghemite — Rutile — Ilmenite

$$CaCO_3 + Mn^{2+} + 0.5O_2 + CO_2 = CaMn(CO_3)_2 \quad (5)$$
Limestone — Kutnahorite

$$CaCO_3 + 2Mn^{2+} + O_2 + 2CO_2 = CaMn(CO_3)_2 + MnCO_3 \quad (6)$$
Limestone — Kutnahorite — Rhodochrosite

Tab. 3
Representative analyses of oxides and spinels in Čučma skarns.

Mineral	Maghemite*	Maghemite*	Maghemite	Ilmenite	Rutile	Pyrophanite	Manganosite	Jacobsite	Jacopsite	Hausmannite	Iwakiite	Iwakiite	Iwakiite
Place	core-Fe skarn	core-Fe skarn	rim-Fe skarn	matrix	matrix	in Mn skarn	in Mn skarn	in Mn skarn	in Mn skarn	in Mn skarn	in Mn skarn	in Mn skarn	in Mn skarn
Stage	1	1	1	1	1	2	2	2	2	2	2	2	2
Process	Metasomatic	Metasomatic	Metasomatic	Metasomatic	Metasomatic	Prog.-metam.	Prog.-metam.	Prog.-metam.	Prog.-metam.	Prog.-metam.	Prog.-metam.	Prog.-metam.	Prog.-metam.
SiO_2	2.96	4.77	0.08	0.47	0.37	0.93	0.00	0.02	0.75	0.00	0.01	0.02	0.01
TiO_2	0.03	0.08	0.08	51.15	92.56	55.44	0.00	0.28	0.14	0.01	0.00	0.09	0.07
Al_2O_3	0.02	0.13	0	0.18	0.12	0.17	0.00	2.89	0.60	0.13	0.38	2.05	1.93
FeO	0.00	0.00	0	43.62	6.08	6.05	0.27	3.00	19.00	2.57	31.51	30.77	31.72
Fe_2O_3	97.58	94.68	98.72	0.00	0.00	0.00	0.00	64.46	65.32	0.00	13.34	6.67	4.44
Cr_2O_3	0.00	0.00	0.03	0.00	0.03	0.04	0.03	0.01	0.00	0.00	0.00	0.00	0.00
MnO	1.69	2.04	0.36	3.64	0.87	36.00	99.67	28.90	13.92	28.43	0.00	0.00	0.00
Mn_2O_3	0.00	0.00	0.00	0.00	0.00	0.00	0.00	0.00	0.00	68.91	54.12	59.80	61.36
MgO	0.52	0.78	0.04	0.04	0.06	0.00	0.00	0.02	0.02	0.00	0.05	0.02	0.01
CaO	0.13	0.22	0.2	0.59	0.00	1.23	0.00	0.01	0.00	0.00	0.01	0.00	0.00
F	0.33	0.28	0.29	0.00	0.00	0.00	0.00	0.00	0.00	0.00	0.00	0.00	0.00
Total	102.93	102.70	99.51	99.70	100.10	99.86	99.97	99.59	99.75	100.05	99.42	99.42	99.54
Si	0.075	0.119	0.002	0.012	0.005	0.023	0.000	0.001	0.029	0.00	0.000	0.001	0.000
Al	0.001	0.004	0	0.005	0.002	0.005	0.000	0.129	0.027	0.01	0.017	0.092	0.086
Ti	0.001	0.002	0.002	0.974	0.945	1.021	0.000	0.008	0.004	0.00	0.000	0.003	0.002
Fe^{2+}	0.000	0.000	0	0.924	0.069	0.124	0.003	0.095	0.610	0.08	1.014	0.977	1.009
Fe^{3+}	1.857	1.781	1.982	0.000	0.000	0.000	0.000	1.840	1.885	0.00	0.386	0.190	0.127
Cr	0.000	0.000	0.001	0.000	0.000	0.001	0.000	0.000	0.000	0.00	0.000	0.000	0.000
Mn^{2+}	0.036	0.043	0.008	0.078	0.010	0.747	0.997	0.929	0.453	0.92	0.000	0.000	0.000
Mn^{3+}	0.000	0.000	0	0.000	0.000	0.000	0.000	0.000	0.000	1.99	1.583	1.726	1.775
Mg	0.020	0.029	0.002	0.002	0.001	0.000	0.000	0.001	0.001	0.00	0.003	0.001	0.001
Ca	0.004	0.006	0.006	0.016	0.000	0.032	0.000	0.000	0.000	0.00	0.000	0.000	0.000
Cations	1.994	1.984	2.003	2.011	1.032	1.953	1.000	3.003	3.009	3.00	3.003	2.990	3.000

* unstechiometry

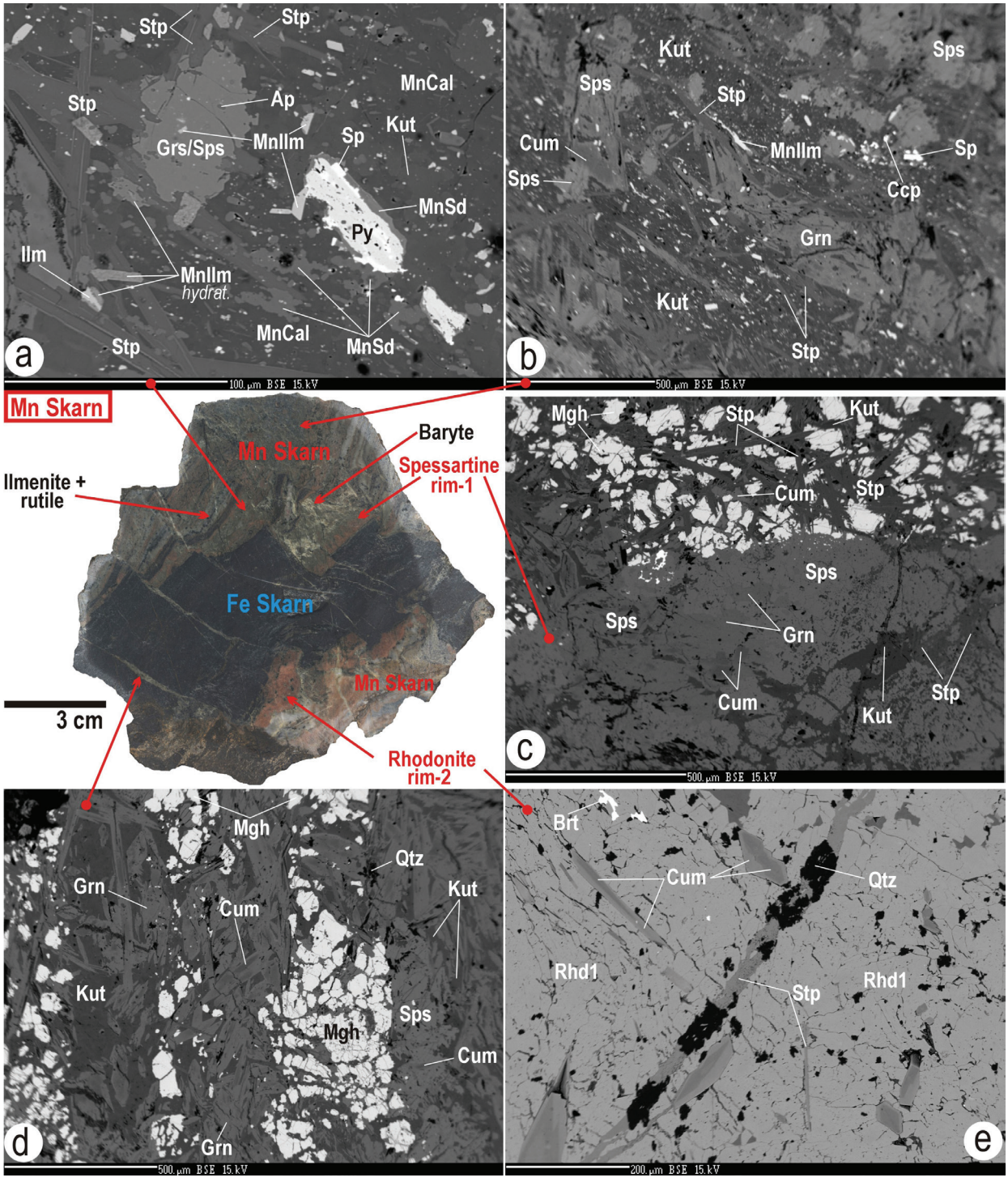

Fig. 4. Successive formation of skarn in the Čučma area. The rose Mn bearing part represents the second prograde and third retrograde metamorphic stages of the skarn evolution. A spessartine margin (rim-1) was formed around the individual segments of Fe skarn, followed by a rhodonite margin (rim-2). The BSE images show places and mineral assemblages in part of Mn skarn. **a, b** – Pyrite (Py) and sphalerite (Sp) are replaced by Mn-rich siderite (MnSd); ilmenite (Ilm) is usually hydrated; cummingtonite (Cum), grunerite (Grn) and chalcopyrite (Ccp) are enclosed in kutnahorite (Kut); prismatic stilpnomelane occurs in kutnahorite, Mn-rich calcite (MnCal) and spessartine (Sps) form the matrix. **c** – rim-1 is formed by the homogeneous spessartine at flanks of maghemite (Mgh) that represents the margin of Fe bearing skarn. The cummungtonite, grunerite and younger stilpnomelane (Stp) independently occur on the contact zone of the Fe skarn. **d** – cracks in the Fe skarn are filled by grunerite, cummingtonite and quartz (Qtz). **e** – rim-2 is composed by the homogeneous rhodonite-1 (Rhd-1) with zonal and prismatic cummingtonite and crack in rhodonite-1 is filled with quartz, stilpnomelne and baryte (Brt).

The reactions above have described first stage with the origin of metasomatic Mn-rich carbonates and Fe bearing skarn. The mineralization of first stage was formed in the process within the chlorite-apatite zone, where the fluorapatite and chlorite represent the indexed minerals. All minerals projections of the chlorite-apatite zone are shown in MgO + FeO – CaO – Fe_2O_3 – MnO tetrahedron (Fig. 10b).

In the chlorite-apatite zone of Gemeric unit there were formed greisen in Dlhá dolina, a part of Hnilec greisen, as well as the Sb-sulfidic-tourmaline-Fe carbonate mineralization in Rozabela vein. The U-rich SedEx mineralization related to the Permian volcanism and the apatite-xenotime mineralization from Čučma belong to this zone, too (Radvanec & Gonda, 2019). The stockwork of apatite-xenotime mineralization is located in metapelite, about 400 m from the studied skarn in Čučma area (Fig. 1).

After the formation of the first stage minerals, the Fe skarn was segmented in brittle-ductile deformation conditions. Subsequently the Fe skarn was metamorphosed in the second stage of its formation (Figs. 2 and 3).

The second stage of skarn formation in prograde metamorphism of amphibolite facies

The second stage of skarn formation metamorphically replaced the unstable Mn carbonates mass, which originated in the older metasomatic stage. This second stage produced the Mn bearing group of garnets, humites, oxides, halides, spinels, olivines, pyroxenoides and amphiboles respectively. This assemblage forms younger and a new part of the skarn. Hence the final formation of the skarn is composed of two parts, the older Fe skarn and the younger Mn skarn. The younger Mn bearing part was formed gradually. At first, segments of Fe skarn were coated by the spessartine during the brittle-ductile deformation and then in the process of ductile deformation a rhodonite bearing rim on the spessartine was formed (Fig. 4). The ductile deformation dominantly controlled the formation of minerals during the second metamorphic stage and therefore the final skarn is mostly fine to medium-grained. The following minerals are arranged by their successive formation in the Mn skarn: spessartine, alleghanyite, pyrophanite, manganosite, kempite, jacobsite, iwakiite, hausmannite, tephroite, Ti-rich tephroite, knebelite, rhodonite-1, rhodonite-2, cummingtonite, grunerite and allanite (Figs. 6, 7 and 9).

The brown-pink Mn-rich garnets are composed by spots of **Ca-rich spessartine** $Sps_{55-72}Grs_{9-34}Adr_{7-19}Alm_{0-3}$ in the **spessartine** $Sps_{69-95}Grs_{0-2}Adr_{3-25}Alm_{0-5}Prp_{0-1}$ mass (Figs. 2b and 5, Tab. 2). Formation of Mn-rich garnets on direct segments of the Fe skarn determine the garnets as one of the first mineral of the metamorphic stage (Fig. 4c). In the kutnahorite matrix the spessartine formed an atoll shapes and in spessartine, relics of Mn-rich chlorite and Mn-rich calcite frequently occur (Figs. 2a, 3 and 4). These relicts of Mn-rich chlorite show formation of spessartine according to the reaction 7.

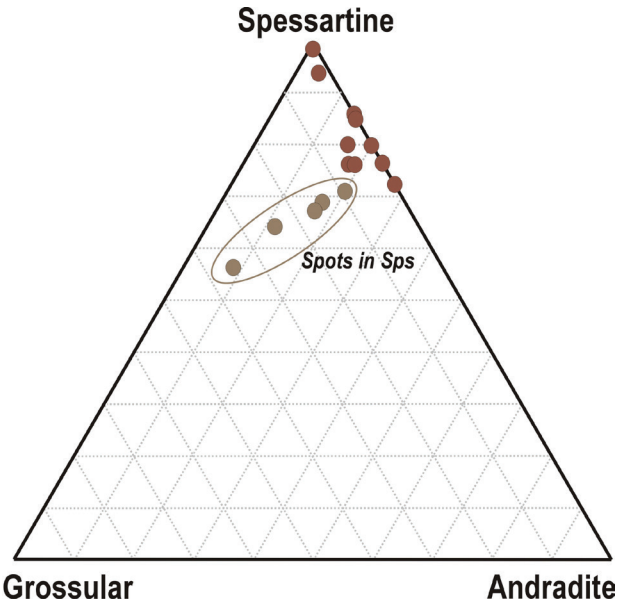

Fig. 5. Chemical composition of Ca rich spessartine and spessartine in triangle diagram grossular-andradite-spessartine end member.

$$\underset{\text{Mn chlorite/pennantite}}{Mn_5Al_2Si_3O_{10}(OH)_8} + 2CO_2 = \underset{\text{Spessartine}}{Mn_3Al_2Si_3O_{12}} + \underset{\text{Rhodochrosite}}{2MnCO_3} + 4H_2O \quad (7)$$

The **alleghanyite** $Mn^{2+}{}_5(SiO_4)_2(OH)_2$ is homogeneous and does not contain any admixtures of other elements. It originated from the rhodochrosite, in which it often forms atoll shapes up to 200 μm in size and/or the alleghanyite forms the oval inclusions in manganosite respectively (Fig. 6, Tab. 2). The alleghanyite is the first mineral binding the SiO_2 fraction from the fluid phase of metamorphic event according to the empiric reaction 8.

$$\underset{\text{Rhodochrosite}}{5MnCO_3} + \underset{\text{fluid phase}}{2SiO_2} + H_2O = \underset{\text{Alleghanyite}}{Mn_5Si_2O_8(OH)_2} + 5CO_2 \quad (8)$$

Pyrophanite $(Fe_{0.23}Mn_{0.78})TiO_3$ contains FeO up to 10.92 wt.% and the Fe/(Fe + Mn) ratio in it ranges from 0.14 to 0.26. The pyrophanite occurs with fluorapatite in the matrix of maghemite and in kutnahorite reaches a size about 20 microns (Figs. 2a and 3b–c). The reaction 9 shows the pyrophanite formation.

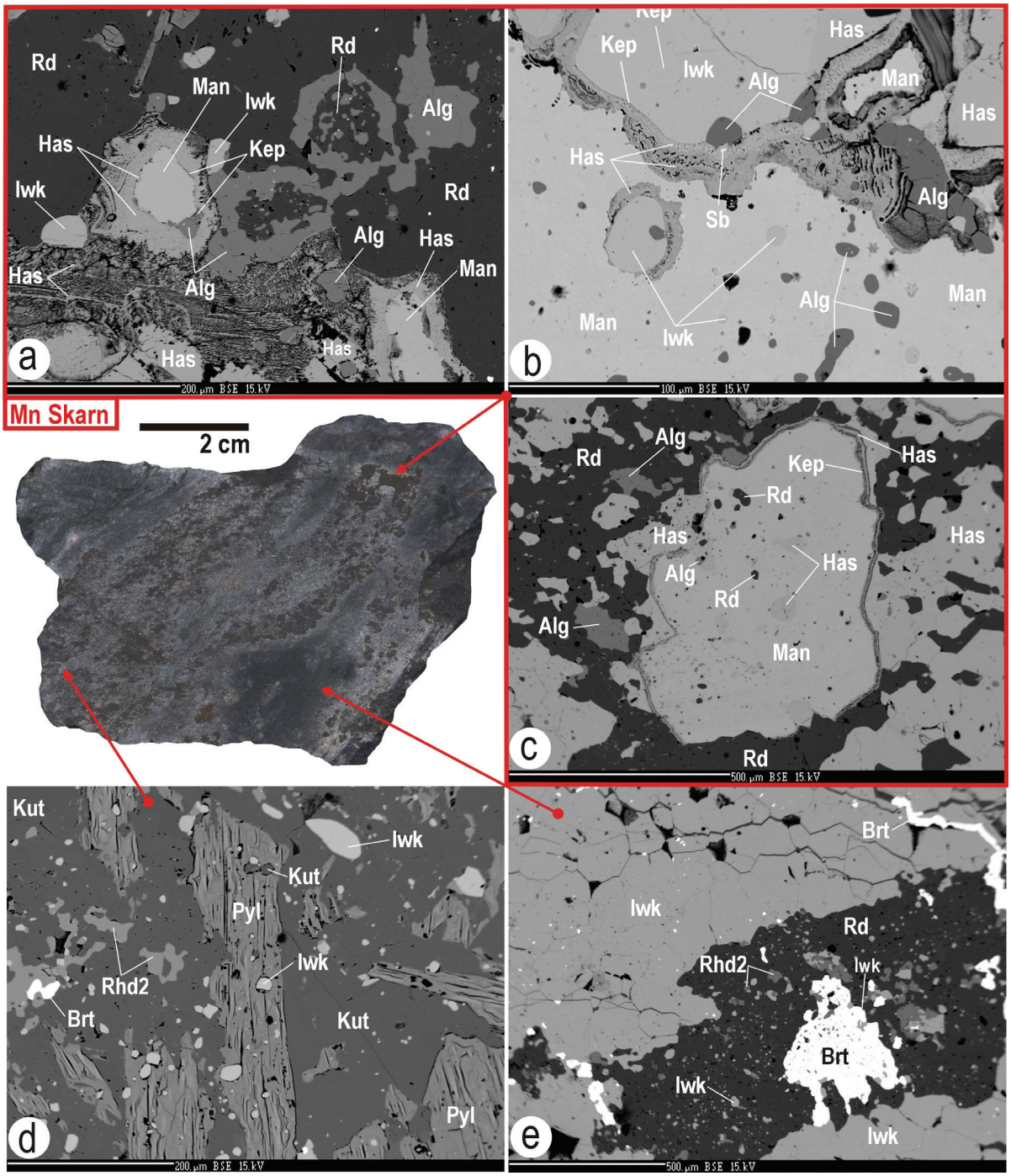

Fig. 6. Broun and black Mn bearing part represents the second prograde metamorphic stages of the skarn evolution. **a** – In rhodochrosite (Rd) spots of alleghanyite (Alg) and iwakite (Iwk) occur and the manganosite (Man) is replaced by kempite (Kep) and by hausmannite (Has) respectively. **b** – In manganosite inclusions of iwakiite and alleghanyite were found. Iwakiite is replaced by hausmannite and rarely native Sb is present in the hausmanite. **c** – In manganosite the relict of rhodochrosite and inclusions of hausmannite were found. **d** – In kutnahorite spots of rhodonite-2 (Rhd-2) the iwakiite occurs and kutnahorite is replaced by pyrolusite (Pyl). **e** – Crack in homogeneous aggregate of iwakiite is filled with baryte (Brt) and in rhodochrosite spots of iwakiite, rhodonite-2 and baryte occur.

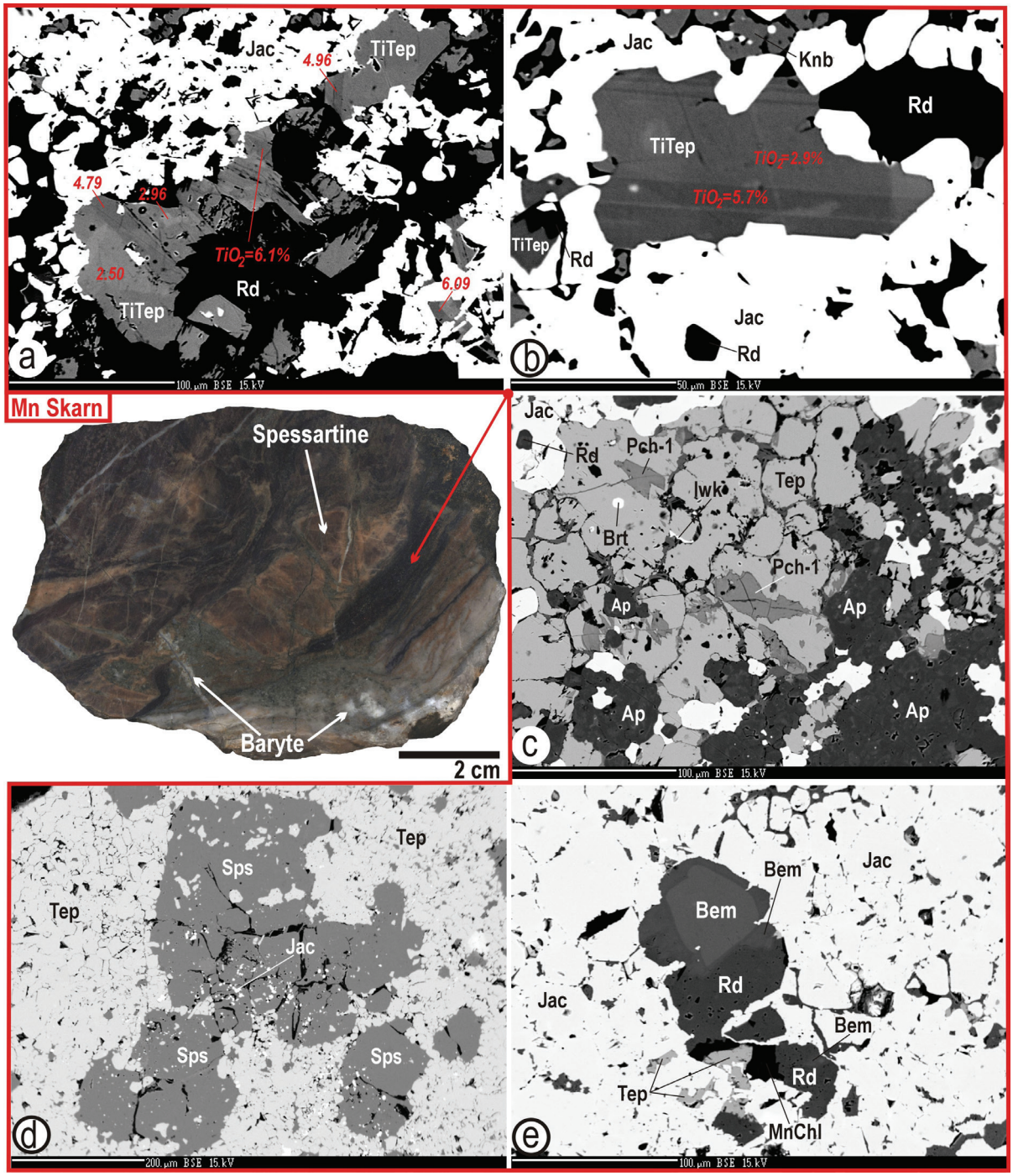

Fig. 7. Mn-rich olivines are located in black part of the skarn and were formed after the spessartine part in prograde metamorphism. Cracks of skarn are filled with baryte. **a, b** – Sectors in Ti-rich tephroite (TiTep) show different TiO_2 content and relics of rhodochrosite (Rd), Ti tephroite and jacobsite (Jac) form the aggregates. **c** – In cracks the tephroite (Tep) is replaced by pyrochroite-1 (Pch-1). Aggregates of tephroite are associated with fluorapatite (Ap), iwakiite (Iwk) and jacobsite (Jac). Baryte (Brt) shows peudoinclusion in tephroite. **d** – Spessartine (Sps) is enclosed in tephroite mass. **e** – Rhodochrosite, bementite (Bem), Mn-rich chlorite (MnChl) and tephroite in jacobsite matrix.

TiO_2 + $MnCO_3$ = $MnTiO_3$ + CO_2 (9)
Rutile Rhodochrosite Pyrophanite

The chemical composition of **manganosite** $(Mn_{0.997}Fe_{0.003})O$ is identical to its end member. It forms a maximum of 5 mm large, emerald green, brown-green to black-green, allotriomorphic and isolated grains or their aggregates. Grains of manganosite have the characteristic glass luster. Decomposition of rhodochrosite by the reaction 10 formed manganosite and reaction 11 shows the possible formation of pyrophanite as well.

$MnCO_3$ = MnO + CO_2 (10)
Rhodochrosite Manganosite

TiO_2 + MnO = $MnTiO_3$ (11)
Rutile Manganosite Pyrophanite

The manganosite is frequently overgrown in a black fine-grained aggregates of rhodochrosite, alleghanyite and **hausmannite** Mn_3O_4 (Fig. 6). Inclusions of **iwakiite** $Fe(Al_{0.09}Fe_{0.13}Mn_{1.78})_2O_4$, alleghanyite, hausmannite are always found in manganosite and relics of former rhodochrosite are still presented in it. The oval inclusions of iwakiite and hausmannite appear as unmixed phases coexisting with the host manganosite (Figs. 6b–c). The grain of manganosite is usually replaced by **kempite** $Mn^{2+}{}_2Cl(OH)_3$ and then by the hausmannite in that order (Figs. 6a–c). In addition to inclusions in manganosite, the hausmannite and iwakiite replaced kutnahorite and rhodochrosite in the matrix of Mn skarn, where hausmannite and iwakiite often in the form of aggregates occur (Fig. 6c–e). Macroscopically these aggregates are fine- to medium-grained (maximum grain size is 2 mm), have a black to black-brown colour, a semi-metallic lustre and on some grains cleavability is well observable. Microscopically, hausmannite and iwakiite grains have an allotriomorphic to hypidiomorphic shape (Fig. 6c–e). The **jacobsite** was also found in that part of Mn skarn and it has the same size and color as hausmannite and iwakiite (Fig. 7). The jacobsite usually forms a mixture in aggregates with Mn-rich olivines and it has a variable chemical formula $(Mn_{0.45\text{-}0.93}Fe^{2+}{}_{0.10\text{-}0.61})(Al_{0.01\text{-}0.13}Fe^{3+}{}_{1.84\text{-}1.94})_2O_4$ (Tab. 3). The empiric reactions from 12 to 19 explain the formation of jacobsite, iwakiite, kempite and hausmannite.

Fe_2O_3 + MnO = $MnFe_2O_4$ (12)
Maghemite Manganosite Jacobsite

$2Fe_2O_3$ + $8MnO$ + O_2 = $4FeMn_2O_4$ (13)
Maghemite Manganosite Iwakiite

Fe_2O_3 + $4MnCO_3$ + $0.5O_2$ = $2FeMn_2O_4$ + $4CO_2$ (14)
Maghemite Rhodochrosite Iwakiite

$2MnO$ + HCl + H_2O = $Mn_2Cl(OH)_3$ (15)
Manganosite Kempite

$5MnO$ + $0.5O_2$ HCl + H_2O = Mn_3O_4 + $Mn_2Cl(OH)_3$ (16)
Manganosite Hausmannite Kempite

$5MnCO_3$ + HCl + H_2O + $0.5O_2$ = Mn_3O_4 + $Mn_2Cl(OH)_3$ + $5CO_2$ (17)
Rhodochrosite Hausmannite Kempite

$2Fe_2O_3$ + Mn_3O_4 + $2MnO$ = $2FeMn_2O_4$ + $MnFe_2O_4$ (18)
Maghemite Hausmannite Manganosite Iwakiite Jacobsite

$FeCO_3$ + Mn_3O_4 = $FeMn_2O_4$ + MnO + CO_2 (19)
Siderite Hausmannite Iwakiite Manganosite

Jacobsite, hausmannite and iwakiite belong to the group of spinels. Projections of their chemical compositions and relationships in comparison to the position of manganosite, rhodochrosite, Mn siderite and maghemite are shown on the tetrahedron (Fig. 10d). The spinels projections revealed their formation by reactions from the source assemblage of manganosite, rhodochrosite, Mn siderite and maghemite. However, the variable projection of the jacobsite compositions, confirm its formation from the former assemblage of hausmannite, iwakiite, maghemite, manganosite and/or rhodochrosite, respectively (Fig. 10d).

Not only spinels but also a complex of Mn-rich olivines were found. The most common is homogeneous **tephroite** $(Mn_{1.86\text{-}1.91}Fe_{0.07\text{-}0.14}Mg_{0.02\text{-}0.04})SiO_4$ that always with jacobsite and rarely with iwakiite form the fine-grained black, sometimes dark brown aggregates in the Mn skarn. The tephroite replaced the former association of spessartine, rhodochrosite, fluorapatite and Mn chlorite in aggregates (Fig. 7). In these aggregates **Ti-rich tephroite** with the variable chemical compositions $(Mn_{1.88\text{-}1.95}Fe_{0.03\text{-}0.09}Mg_{0.03\text{-}0.06})(Fe^{3+}{}_{0\text{-}0.03}Ti_{0\text{-}0.16}Si_{0.84\text{-}0.98})O_4$ also occurs. It is black and reaches a size of up to 250 μm. The Ti-rich tephroite usually replaced former rhodochrosite and is always enclosed in the matrix of jacobsite. In the Ti-rich tephroite, an oval inclusions of homogeneous tephroite is rarely enclosed and these inclusions are free of TiO_2. Each grain of Ti-rich tephroite consists of sectors that are visible in BSE images only at high acceleration of 100 nA. Individual sectors were quantified by TiO_2 content. In the sector with the lowest content, TiO_2 ranges from 0.14 to 0.32 wt.%, in the next sector the range is from 1.44 to 2.96 and the sector with a maximum TiO_2 content ranges from 4.83 to 6.22 (Fig. 7a–b). In the chemical formula of the sectors, the Ti content ranges from 0.008 to 0.159 (apfu) and Si from 0.842 to 0.981 respectively. It shows that the Ti content substituted Si and an immiscibility gap between the individual sectors are determined by different contents of Ti and Si in that substitution (Fig. 8). The $\mathbf{Ti^{4+} = Si^{4+}}$ is a new substitution in the chemical formula of olivine, however according to the olivine stoichiometry this substitution have to be improved by adding a low Fe^{3+} content (apfu) to the Ti component. The Fe^{3+} correction was locally calculated for the first two sectors within the range 0.014–0.057 (apfu) and in the sector with the highest Ti content, there is the substitution of Ti versus Si without an effect of Fe^{3+} (Tab. 4). The $Ti^{4+} = Si^{4+}$ substitution was formed between end members of tephroite and rutile by the empiric reactions 22–23.

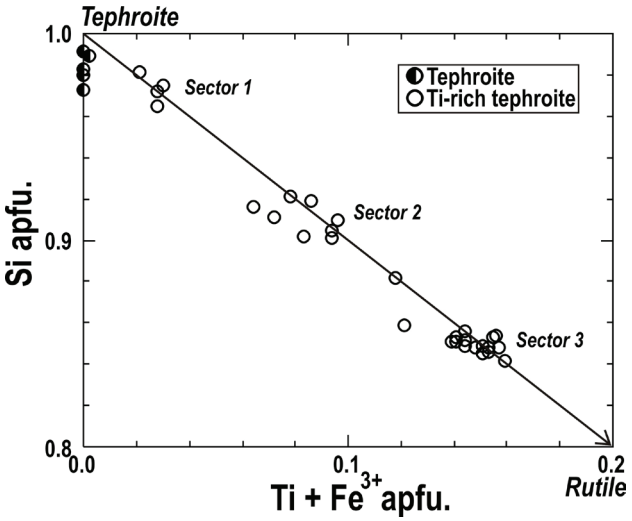

Fig. 8. The content of Si versus Ti + Fe^{3+} between end members of tephroite and rutile shows a new substitution in the olivine group composed of different immiscible sectors in Ti-rich tephroite.

Homogeneous **knebelite** $(Mn_{1.66}Fe_{0.30\text{-}0.33}Mg_{0.06})Si_{0.99\text{-}0.98}O_4$ is the next from the group of olivines present in the Mn skarn. The Fe/(Fe + Mg) ratio in knebelite is 0.84–0.85 and Fe/(Fe + Mg + Mn) ratio is to 0.15–0.16 (Tab. 4). The knebelite of a dark grey to steel color replaces rhodochrosite and fluorapatite. Together with rhodonite, spessartine and bementite form aggregates where knebelite reaches a size of 500 μm. In these aggregates two population of homogeneous rose pink **rhodonite-1** $(Mn_{0.74}Fe_{0.09\text{-}0.13}Mg_{0.02\text{-}0.030}Ca_{0.10\text{-}0.12}Fe^{3+}{}_{0.02\text{-}0.04})Si_{0.98\text{-}0.99}O_3$ and pink **rhodonite-2** $(Mn_{0.87\text{-}0.89}Fe_{0\text{-}0.02}Mg_{0.02\text{-}0.030}Ca_{0.08\text{-}0.10}Fe^{3+}{}_{0.03\text{-}0.04})Si_{0.97\text{-}0.99}O_3$ form the matrix, where the knebelite is present respectively (Fig. 9). In the aggregates those two modes of rhodonite unmixed each other and their variation in the molecular components are as follows (in mol.%): rhodonite-1 – 73.72–74.09 $MnSiO_3$, 9.97–12.25 $CaSiO_3$, 9.10–12.5 $FeSiO_3$, 2.11–3.07 $MgSiO_3$; rhodonite-2 – 86.60–88.50 $MnSiO_3$, 8.02–9.54 $CaSiO_3$, 0–1.80 $FeSiO_3$, 2.12–2.51 $MgSiO_3$. The wollastonite ($CaSiO_3$), ferrosilite ($FeSiO_3$) and enstatite $MgSiO_3$ components are on average higher in the rhodonite-1, while the $MnSiO_3$ molecule is higher in rhodonite-2. The wollastonite molecule of both rhodonites ranges from 8.02 to 12.25 (mol.%) and $MnSiO_3$ ranges from 73.72 to 88.50 (mol.%). If a Mn-rich pyroxenoide has that range of $MnSiO_3$ molecule, the wollastonite component have to be ranged from 2.7 to 5.5 (mol.%) in the field of pyroxmangite because compositional boundaries between rhodonite and pyroxmangite is determinate by the wollastonite component (Momoi, 1964; Brown et al., 1980). However both studied pyroxenoides are clearly in the field of rhodonite where the wollastonite molecule ranges from 8.02 to 12.25 (mol.%; Tab. 4).

In the rhodonite-1, the Fe/(Fe + Mg) ratio ranges from 0.75 to 0.86 and Fe/(Fe + Mg + Mn) from 0.11 to 0.13. The rhodonite-1 and knebelite have values of both ratios approximately the same, indicating the coexistence in their common aggregates (Fig. 9). The rhodonite-2 usually forms irregular grains in rhodochrosite (Fig. 6e). The Fe content in the chemical formula of the rhodonite-2 is

Tab. 4
Representative analyses of olivines and rhodonite in Čučma skarns.

Mineral	Knebelite	Tephroite	Ti tephroite	Ti tephroite	Ti tephroite	Ti tephroite	Ti tephroite	Ti tephroite	Ti tephroite	Ti tephroite	Ti tephroite	Rhodonite 1	Rhodonite 1	Rhodonite 2	Rhodonite 2
Place	Mn skarn	Mn skarn	Sector 1	Sector 1	Sector 2	Sector 2	Sector 2	Sector 3	Sector 3	Sector 3	Sector 3	Mn skarn	Mn skarn	Mn skarn	Mn skarn
Stage	2	2	2	2	2	2	2	2	2	2	2	2	2	2	2
Process	Prog.-metam.	Prog.-metam.	Prog.-metam.	Prog.-metam.	Prog.-metam.	Prog.-metam.	Prog.-metam.	Prog.-metam.	Prog.-metam.	Prog.-metam.	Prog.-metam.	Prog.-metam.	Prog.-metam.	Prog.-metam.	Prog.-metam.
SiO_2	29.59	28.54	29.40	29.29	27.12	26.81	25.88	25.19	24.91	24.98	24.68	45.88	45.93	45.15	45.23
TiO_2	0.00	0.00	0.08	0.31	2.50	2.96	4.61	5.09	5.40	5.78	6.18	0.00	0.00	0.01	0.01
Al_2O_3	0.00	0.00	0.00	0.02	0.00	0.00	0.00	0.00	0.00	0.01	0.00	0.00	0.02	0.00	0.19
Cr_2O_3	0.04	0.03	0.00	0.00	0.00	0.00	0.02	0.00	0.00	0.00	0.03	0.00	0.00	0.00	0.00
FeO	10.85	2.47	4.87	1.83	3.06	3.00	4.83	2.28	2.24	2.75	0.00	8.23	7.11	2.19	1.88
Fe_2O_3	0.00	0.00	0.00	0.54	0.00	0.78	0.00	0.56	0.00	0.00	0.00	0.00	0.00	0.00	0.00
MnO	58.50	68.10	65.33	67.71	67.37	65.94	63.72	65.05	65.19	64.62	64.95	40.72	40.71	48.72	48.08
MgO	1.07	0.72	0.36	0.56	0.48	0.37	0.43	1.36	1.38	1.38	0.56	0.77	0.95	0.70	0.66
CaO	0.03	0.02	0.05	0.03	0.03	0.03	0.04	0.05	0.03	0.04	0.05	4.33	5.35	3.61	4.15
Na_2O	0.02	0.00	0.00	0.00	0.03	0.01	0.00	0.00	0.01	0.00	0.02	0.03	0.00	0.01	0.00
K_2O	0.00	0.00	0.00	0.01	0.00	0.00	0.00	0.00	0.00	0.00	0.00	0.01	0.01	0.01	0.00
F	0.00	0.00	0.00	0.00	0.00	0.00	0.00	0.00	0.00	0.00	0.00	0.00	0.00	0.00	0.00
Cl	0.00	0.00	0.00	0.00	0.00	0.00	0.00	0.00	0.01	0.00	0.00	0.06	0.01	0.02	0.00
Total	100.11	99.87	100.09	100.30	100.59	99.90	99.53	99.58	99.17	99.56	99.57	100.03	100.11	100.44	100.20
Si	0.991	0.968	0.989	0.981	0.916	0.910	0.882	0.856	0.851	0.848	0.842	0.985	0.982	0.969	0.971
Al	0.000	0.000	0.000	0.001	0.000	0.000	0.000	0.000	0.000	0.000	0.000	0.000	0.001	0.000	0.005
Ti	0.000	0.000	0.002	0.008	0.064	0.076	0.118	0.130	0.139	0.148	0.159	0.000	0.000	0.000	0.000
Fe^{3+}	0.000	0.000	0.000	0.013	0.000	0.020	0.000	0.014	0.000	0.000	0.000	0.031	0.036	0.039	0.034
Fe^{2+}	0.304	0.070	0.137	0.051	0.086	0.085	0.138	0.065	0.064	0.078	0.088	0.117	0.091	0.000	0.000
Cr	0.001	0.001	0.000	0.000	0.000	0.000	0.001	0.000	0.000	0.000	0.001	0.000	0.000	0.000	0.000
Mn	1.658	1.956	1.861	1.921	1.928	1.895	1.839	1.872	1.886	1.858	1.878	0.741	0.737	0.885	0.874
Mg	0.053	0.036	0.018	0.028	0.024	0.019	0.022	0.069	0.070	0.070	0.028	0.025	0.030	0.023	0.021
Ca	0.001	0.001	0.002	0.001	0.001	0.001	0.001	0.002	0.001	0.001	0.002	0.100	0.123	0.083	0.095
Na	0.001	0.000	0.000	0.000	0.002	0.001	0.000	0.000	0.001	0.000	0.001	0.001	0.000	0.001	0.000
K	0.000	0.000	0.000	0.000	0.000	0.000	0.000	0.000	0.000	0.000	0.000	0.000	0.000	0.000	0.000
Cations	3.009	3.032	3.009	3.004	3.021	3.007	3.001	3.008	3.012	3.003	2.999	2.000	2.000	2.000	2.000

calculated as Fe^{3+} hence the Fe/(Fe + Mg) and Fe/(Fe + Mg + Mn) ratios are 0 (Tab. 4). In addition, rhodonite-1 forms the outer rim-2 of spessartine rim-1 and both rims were gradually formed at the Fe skarn (Fig. 4). The knebelite was not found in those rim-2 of rhodonite-1 however the prismatic **cummingtonite** is in the rhodonite-1 frequently occurring and cracks in that rhodonite-1 are filled with quartz, stilpnomelane and baryte (Fig. 4e). Found cummingtonite is zoned and in its core the Fe/(Fe + Mg) ratio ranges from 0.47 to 0.56 and the Fe/(Fe + Mg + Mn) is from 0.35 to 0.39. The rim of cummingtonite shows higher values of Fe/(Fe + Mg), which ranges from 0.69 to 0.71 and the Fe/(Fe + Mg + Mn) is from 0.48 to 0.49. Towards the outer rim-2 and in cracks of Fe skarn the core of cummingtonite was frequently replaced by the grunerite (Fig. 4d). In this position the grunerite has the same value of Fe/(Fe + Mg) = 0.68–0.72 as the rim of cummingtonite from those zoned grains, but values of Fe/(Fe + Mg + Mn) = 0.60–0.64 are higher in grunerite that had growing on cummingtonite (Tab. 2). Grunerite, frequently occurs with a mix of kutnahorite and spessartine, is prismatic, homogeneous and younger than cummintonite (Fig. 4b–c).

The origin of tephroite, Ti-rich tephroite, knebelite, rhodonite-1, rhodonite-2, cummingtonite and grunerite were successively formed by reactions of 20–32 where the SiO_2 component determined and controled the crystalline system of that assemblage.

The origin of minerals in second metamorphic stage is described by the relationships of minerals and by empiric reactions 7–32. Some reactions were confirmed experimentally and this allowed to determine the P-T conditions of Mn skarn formation in the Čučma area. Using the reaction 21 and experimental study of the stability field between manganosite and tephroite the formation of tephroite was calculated in the range from 640 to 700 °C according to Beardi & Tracy (2002). The pair of rhodonite-1 ($CaSiO_3$ = 9.97–12.25 mol.%) rhodonite-2 ($CaSiO_3$= 8.02–9.54 mol.%) were formed in $MnSiO_3$–$CaSiO_3$ system by the reaction 27. Contents of $CaSiO_3$ in rhodonites show their crystallization in the stability field of rhodonite at over 600 °C and pressure lower than 4 kbar (Ito, 1972; Broun et al., 1980; Akimoto & Syono, 1972). According to the experiments with composition of grunerite $Fe_7Si_8O_{22}(OH)_2$ molecule in the Fe-rich amphibole, an thermo-barometer was determined by Fonarev et al. (1977) and Gilbert et al. (1982). In studied grunerite the molecule of $Fe_7Si_8O_{22}(OH)_2$ ranges from 58.84 to 64.06 mol.% and using that thermo-barometer the grunerite formation reached 625–675 °C in the pressure limit from 2 to 4.9 kbar. Evaluating the above data, the P-T formation of Mn skarn around 600–650 °C and pressure from 2 to 5 kbars in the amphibolite facies were deduced.

$$MnO + SiO_2 = MnSiO_3 \quad (20)$$
Manganosite — Rhodonite

$$2MnO + SiO_2 = Mn_2SiO_4 \quad (21)$$
Manganosite — Tephroite

$$5MnO + 2TiO_2 + SiO_2 = 2Mn_2(Si,Ti)O_4 + MnTiO_3 \quad (22)$$
Manganosite — Rutile — Ti-rich tephroite — Pyrophanite

$$5MnCO_3 + 2TiO_2 + SiO_2 = 2Mn_2(Si,Ti)O_4 + MnTiO_3 + 5CO_2 \quad (23)$$
Rhodochrosite — Rutile — Ti-rich tephroite — Pyrophanite

$$2MnCO_3 + SiO_2 = Mn_2SiO_4 + 2CO_2 \quad (24)$$
Rhodochrosite — Tephroite

$$2(MnFe)CO_3 + SiO_2 = (MnFe)_2SiO_4 + 2CO_2 \quad (25)$$
Mn siderite — Knebelite

$$Mn_2SiO_4 + SiO_2 = 2MnSiO_3 \quad (26)$$
Tephroite — Rhodonite

$$MnCO_3 + SiO_2 = MnSiO_3 + CO_2 \quad (27)$$
Rhodochrosite — Rhodonite

$$MnO + SiO_2 = MnSiO_3 \quad (28)$$

Manganosite Rhodonite

$$MnCO_3 + MnSiO_3 = Mn_2SiO_4 + CO_2 \quad (29)$$

Rhodochrosite Rhodonite Tephroite

$$9(Fe,Mg,Mn)CO_3 + 9SiO_2 + H_2O = (Fe,Mg,Mn)_7Si_8O_{22}(OH)_2 + (Fe,Mg,Mn)_2SiO_4 + 9CO_2 \quad (30)$$

Sideroplesite/Mn Siderite Cummingtonite Knebelite

$$7(Fe,Mg,Mn)CO_3 + 8SiO_2 + H_2O = (Fe,Mg,Mn)_7Si_8O_{22}(OH)_2 + 7CO_2 \quad (31)$$

Sideroplesite/Mn siderite Grunerite/Cummingtonite

$$7Ca(Fe,Mg,Mn)(CO_3)_2 + 8SiO_2 + H_2O = (Fe,Mg,Mn)_7Si_8O_{22}(OH)_2 + 7CaCO_3 + 7CO_2 \quad (32)$$

Ankerite/Kutnahorite Grunerite/Cummingtonite Mn Calcite

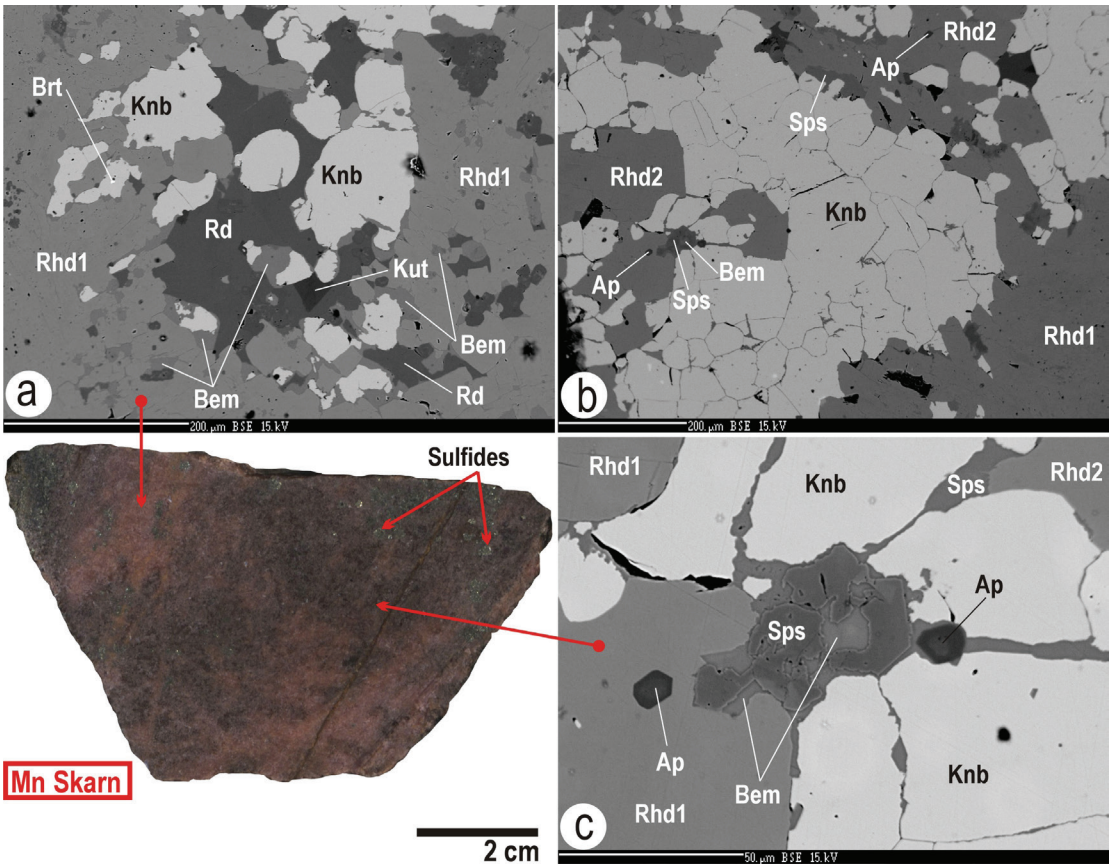

Fig. 9. Rose part of Mn skarn is composed by aggregates of two modes of rhodonite (Rhd-1, Rhd-2), knebelite (Knb), bementite (Bem) and by relicts of rhodochrosite (Rd), kutnahorite (Kut) and fluorapatite (Ap). Amphibolite facies.

Third stage of skarn formation in retrograde metamorphism of stilpnomelane-chlorite zone

Third stage of skarn formation hydrated and replaced the unstable minerals of previous two stages by Si, Ba, H_2S and H_2O bearing fluid phase. Mineral assemblage of the third stage are: Ca-rich spessartine, bementite, pyrochroite, quartz, pyrolusite, baryte, chlorite and stilpnomelane. This mineral association was formed in descending order with decreasing temperature from amphibolite facies to the stilpnomelane-chlorite zone in retrograde metamorphism. The onset of retrograde phase is indicated by spots of **Ca-rich spessartine** in the matrix of spessartine. Its formation is described by reaction 33 and detailed position of Ca-rich spessartine is given in the previous text (Figs. 2b and 5).

The **bementite** usually replaced rhodochrosite, rhodonite-1 and spessartine (Figs. 2a, 7e and 9a-c). Reactions 33–35 show its formation. The forming of **bementite** has two modes of occurrence and its chemical composition depends on the composition of the former mineral that bementite has replaced. The bementite $(Fe_{0.32-0.34}Mg_{0.16-0.22})Mn_{7.47-7.55}(Al_{0.05-0.08}Si_{5.90-5.95})O_{15}(OH)_{10}$, which replaced the spessartine, has a uniform Fe/(Fe + Mg + Mn) ratio 0.04 (Figs. 2a, 9c). However in the bementite that replaced the rhodochrosite and rhodonite-1 the ratio ranges from 0.09 to 0.18 and that bementite is Fe-rich $(Ca_{0.01-0.07}Fe_{0.68-1.47}Mg_{0.17-0.54})Mn_{6.26-6.80}(Al_{0-0.50}Si_{5.50-6.08})O_{15}(OH)_{10}$ (Figs. 7a, 9a-b; Tab. 4). In the case of empiric reaction 34, where bementite formation originated from the association of Mn-rich siderite, rhodochrosite and alleghanyite, the increased Fe content in that bementite come from the Mn-rich siderite source. Like bementite, the **pyrochroite** has two modes of occurrence as well, depending on the composition of minerals that the pyrochroite replaced. The pyrochroite-1 $(Si_{0.07}Fe_{0.02}Mn^{2+}_{0.82})(OH)_2$ has the Fe/(Fe + Mg + Mn) ratio of 0.03 like bementite that replaced the spessartine (0.04), indicating coexistence of both minerals and as well as indicating the identical composition of H_2O bearing fluid phase, from which they were formed. The pyrochroite-1 usually replaced the host tephroite along cracks and therefore the pyrochroite-1 contains variable SiO_2 in the range from 5.24 to 5.43 wt.%. The SiO_2 content in pyrochroite-1 comes from the replaced tephroite (Fig. 7a). In the pyrochroite-2 $(Ca_{0.08-0.09}Mg_{0.04}Fe_{0.01-0.07}Mn^{2+}_{0.79-0.85})(OH)_2$ the Fe/(Fe + Mg + Mn) ratio ranges from 0.01 to 0.08. That pyrochroite-2 frequently replaces the former Mn-rich carbonates and spessartine and this is why pyrochroite-2 is free of SiO_2 (Fig. 2c, Tab. 2). Empirical reactions 33 and 36–38 describe the formation of pyrochroite.

The **pyrolusite** $(Mn^{4+})O_2$ create a homogeneous a black mass, usually amorphous, often with a granular, fibrous or columnar structure, sometimes is forming a reniform crusts on the individual Mn skarn segments (Fig. 2). The pyrolusite preferably replaces the Mn-rich carbonates in the Mn skarn and was formed according to the reaction 39 (Fig. 6d). Homogeneous **baryte** $BaSO_4$ frequently occurs in Mn skarn however no baryte was found in the part of Fe skarn (Figs. 4b, 6d–e and 7c). The baryte position to other minerals depends on the cut by which the thin section was made. Therefore, it sometimes takes the form of pseudo inclusion (Figs. 4e, 7c and 9a). Elsewhere, baryte occurs in the form of agglomerates or fills cracks in the Mn skarn (Figs.6d–e and 7). Other minerals of the third stage of skarn formation are the **chlorite and stilpnomelane**. The stilpnomelane forms prismatic grains namely in cracks and it is rich of Mn with the Mn/(Fe + Mg + Mn) ratio about 0.74 in the matrix of Mn bearing part of skarn. The stilpnomelane occurs also at the rim in Fe bearing part of skarn, where is occurs with maghemite. In stilpnomelane the Mn/(Fe + Mg + Mn) ratio is 0.11 (Fig. 4). The occurrence of stilpnomelane in Fe and Mn skarns shows the different composition of stilpnomelane formulas according to the Mn/(Fe + Mg + Mn) ratio. These ratios are controlled by the place of the stilpnomelane formation however their formulas always show the ferric base in both mode of stilpnomelanes occurrence (Tab. 2). The ferric contents and a different Mn ratio precludes the possibility that stilpnomelane is a coexisting mineral with grunerite or cummingtonite.

Chlorite and stilpnomelane are the indexed minerals of the stilpnomelane-chlorite zone, which ranges within 320–370 °C in the Gemeric unit (Radvanec & Gonda, 2019). In skarn formation on Čučma locality the stilpnomelane-chlorite zone is the retrograde metamorphic phase. The third retrograde stage of skarn formation in stilpnomelane-chlorite zone in Čučma area is described by reactions 33–39 and by projection of minerals in tetrahedrons (Fig. 10).

$$\underset{\text{Mn chlorite}}{(Fe,Mg)Mn_4Al_2Si_3O_{10}(OH)_8} + \underset{\text{Kutnahorite}}{CaMn(CO_3)_2} + \underset{\text{Alleghanyite}}{Mn_5Si_2O_8(OH)_2} + 4SiO_2 + H_2O =$$
$$\underset{\text{Ca-rich Spessartine}}{CaMn_2Al_2Si_3O_{12}} + \underset{\text{Bementite}}{(Fe,Mg)Mn_7Si_6O_{15}(OH)_{10}} + \underset{\text{Pyrochroite-1}}{Mn^{2+}(OH)_2} + 2CO_2 \quad (33)$$

$$\underset{\text{Mn Siderite}}{2(Fe,Mg,Mn)CO_3} + \underset{\text{Rhodochrosite}}{MnCO_3} + 4SiO_2 + \underset{\text{Alleghanyite}}{Mn_5Si_2O_8(OH)_2} + 4H_2O = \underset{\text{Bementite}}{(Fe,Mg)Mn_7Si_6O_{15}(OH)_{10}} + 3CO_2 \quad (34)$$

$$\underset{\text{Rhodochrosite}}{8MnCO_3} + 6SiO_2 + 5H_2O = \underset{\text{Bementite}}{Mn_8Si_6O_{15}(OH)_{10}} + 8CO_2 \quad (35)$$

$$\underset{\text{Tephroite}}{Mn_2SiO_4} + 2H_2O = \underset{\text{Pyrochroite-1}}{2Mn^{2+}(OH)_2} + \underset{\text{Quartz}}{SiO_2} \quad (36)$$

$$\underset{\text{Rhodochrosite}}{MnCO_3} + H_2O = \underset{\text{Pyrochroite-2}}{Mn^{2+}(OH)_2} + CO_2 \quad (37)$$

$$MnO + H_2O = Mn^{2+}(OH)_2 \quad (38)$$
Manganosite — Pyrochroite-2

$$2MnCO_3 = Mn_2O_4 + 2CO_2 \quad (39)$$
Rhodochrosite — Pyrolusite

The skarn geochemistry in comparison to reference granites and position of skarn to related metamorphic-magmatic-hydrothermal mineralization

Three representative samples of skarns were analyzed to elements including REE contents. First sample, representing the Fe skarn, is rich of maghemite, second sample, representing metasomatic part has a predominance of rhodochrosite – kutnahorite and third sample representing Mn skarn, includes spinels, Mn/Ti olivines, rhodonite and amphiboles (Tab. 5). According to the procedure of Sun and McDonough (1989), the normalized REE contents distinguish two groups of these skarn samples. First group of Fe bearing part with maghemite and the metasomatic Mn skarn section with a predominance of rhodochrosite and kutnahorite are identically compared with the upper crust. It means that the Mn bearing fluid phase of chlorite-apatite zone that replaced the former limestone to create the Mn-rich carbonates and maghemite was derived from the upper crust source (Fig. 11). Second group represents the metamorphic overprint and formation of Mn skarn in the prograde amphibolite facies and retrograde metamorphic stage in stilpnomelane-chlorite zone. These metamorphic stages are in good agreement with the formation, influenced by the fluid phase, which has originated from the primitive mantle (Fig. 11). Both groups of the "upper crust" and the "influence of the mantle" were also determined in others mineralizations that were formed during the Permian metamorphic-magmatic-hydrothermal (MMH) cycle in Paleo-Gemeric region. The "upper crust" mineralization is in good accordance of the Lower and Middle Permian events and the "influence of the mantle" was found in mineralizations which were formed in the Middle and Upper Permian (Radvanec & Gonda, 2019).

The Permian metamorphic-magmatic cycle is represented by individual facies of orogenic metamorphism, by S-type granites and by their effusive equivalents (andesite, dacite, rhyolite, basalt) on the surface (Grecula et al., 2009; Radvanec & Grecula, 2016; Vozárová & Vozár, 1988). Permian period is characterized by the low- to medium pressure metamorphism with high temperature gradients in the range of 40–50 °C/km. This extreme overheating of the Paleo-Gemeric region in Permian caused regional metamorphism which culminated with S-type anatectic granite magmatism in amphibolite facies (Radvanec et al., 2007, 2009, 2017; Radvanec & Grecula, 2016; Radvanec

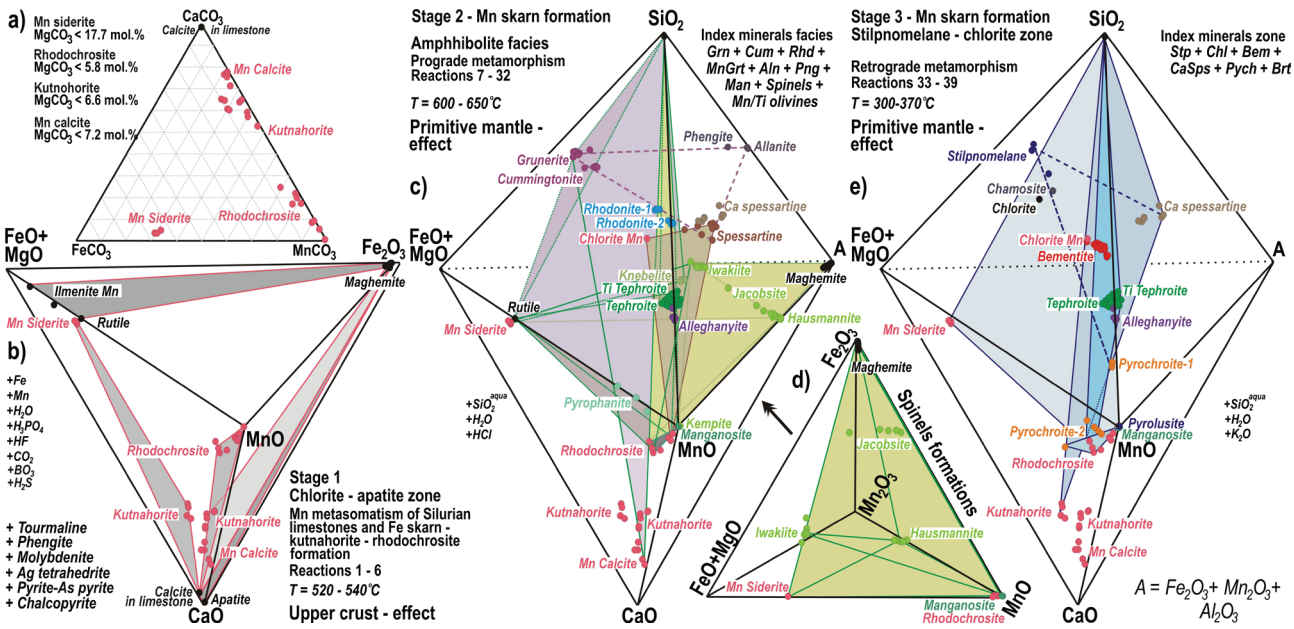

Fig. 10. Projections of minerals according to three successive stages of Fe and Mn skarns formation in triangle diagrams and in individual tetrahedrons that are united by the common base. **a** – Classification of carbonates. **b** – Minerals projection of chlorite-apatite zone in first metasomatic stage and related empiric reactions. **c** – Minerals projection of prograde metamorphism of amphibolite facies in second stage and related empiric reactions of the skarn formation. **d** – Spinels projections in tetrahedron related in the second stage of the skarn formation. **e** – Minerals projection of retrograde metamorphism in third stage of stilpnomelane-chlorite zone and related empiric reactions of the skarn formation.

& Németh, 2018). The Permian MMH cycle was a product of the final (collisional) stage of earlier subduction and related to the volcanic arc magmatism, having mentioned two modes: (1) Older cycle (281–273 Ma) producing porphyric granites of volcanic arc (VAG), cassiterite greisen, apatite-xenotime stockworks, maghemite-cassiterite-ankerite skarn, as well as andesite (K-CAB) and U-rich SedEx mineralization in the North-Gemeric zone, having source in the upper crust. (2) Younger cycle (263–251 Ma) had the mantle influence and produced differentiated syn-collisional granites (syn-COLG) with cassiterite-tourmaline-Fe, as well as tourmaline-molybdenite-Fe carbonates greisens, maghemite-cassiterite-Fe carbonate-FeZnCu-BiTeIn sulfides bearing skarn and related Mg-Fe metasomatites, Sb-rich sulfides-tourmaline-Fe carbonates veins, siderite-sulfides veins and rhyolite (K-CAB) with related U Mo-Cu-rich SedEx breccia. According to the Re-Os dating of molybdenite and cassiterite there has been found that mineralization in the Permian cycle formed within an interval of 268–256 Ma and lasted 12 Ma (Kohút & Stein, 2005; Kohút et al., 2013). The igneous cycle lasted 30 Ma from 281 to 251 Ma (Radvanec et al., 2004, 2007, 2009, 2010; Radvanec & Grecula, 2016; Vozárová & Vozár, 1988; Vozárová et al., 2015; Radvanec & Gonda, 2019). The influence of primitive mantle in younger magmatic cycle in the period of 269–251 Ma indicates that in this period the subducted rocks were melted in deeper part of subduction zone together with the mantle. This deep-located melting in the mantle results in differentiated granitic melt with the mantle influence, found in medium- and fine-grained granites and their effusive equivalent – rhyolite (Radvanec et al., 2007, 2009, 2017; Radvanec & Grecula, 2016; Radvanec & Gonda, 2019; Fig. 11).

Contents of elements in those three parts of skarn in Čučma locality were normalizing by the reference contents of anatectic S-type granites concordantly with the methodology described above. Along with granites the related mineralization were formed in the hotlines above the subduction zone during the Permian development of Paleo-Gemericum according to the MMH cycle of Radvanec et al. (2009) and Radvanec & Gonda (2019). This MMH cycle shows the development of

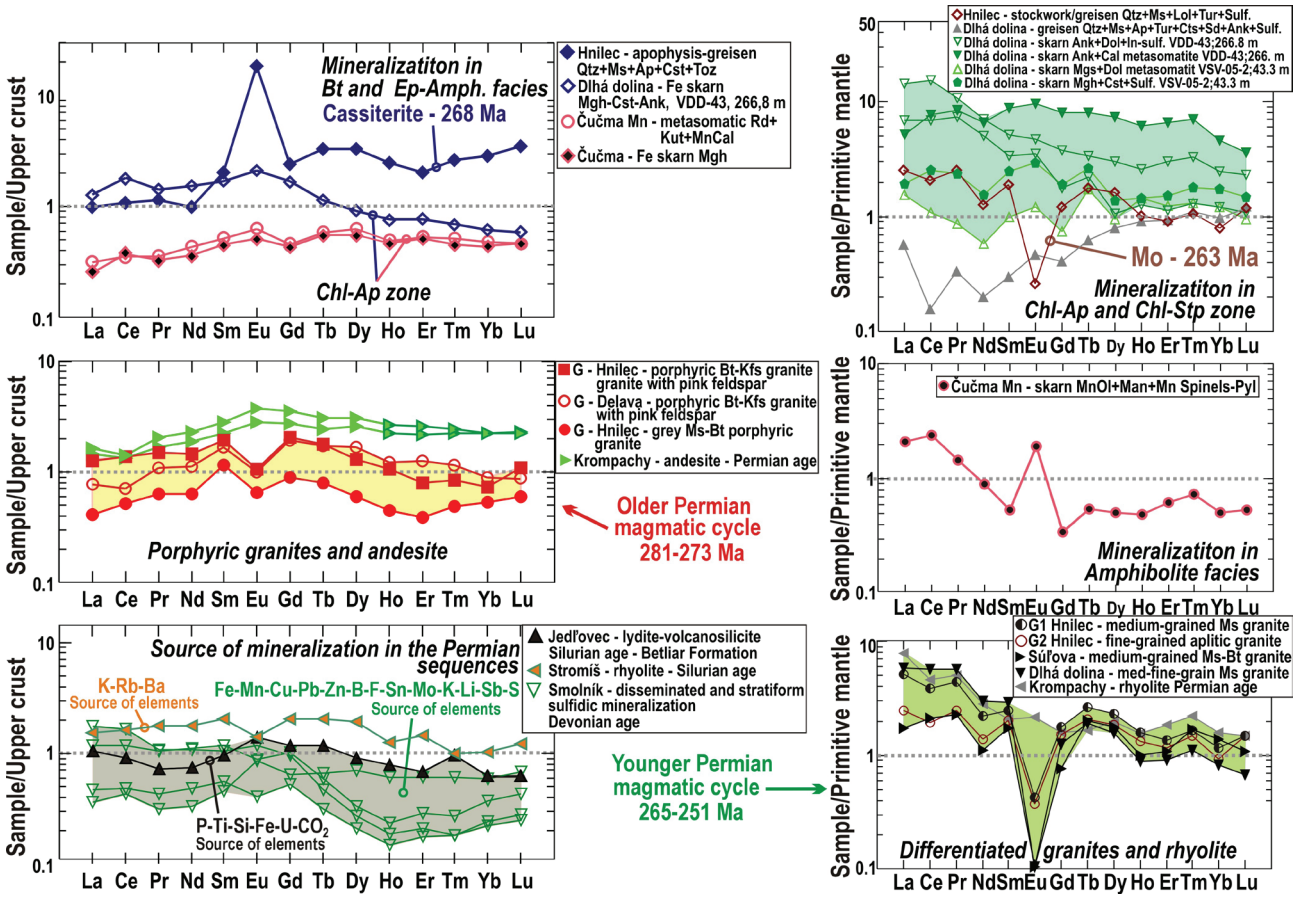

Fig. 11. Classification of Permian metamorphic-magmatic-hydrothermal cycle with the REE contents normalization and related ages. First group is classified by the REE normalization as a group identical with the upper crust and having Lower to Middle Permian age. Second group is according to contents and REE normalization identical with primitive mantle, having Middle to Upper Permian age. Skarns and comparable rocks are reported by Radvanec & Gonda (2019) and in Table 5. Normalization on upper crust and primitive mantle is according to Sun & McDonough (1989).

hydrothermal mineralization from the deep-rooted zone of the amphibolite and epidote-amphibolite facies, including anatectic melting to volcanic-exhalation mineralization of SedEx on the surface. To identify source rocks that have primary anomalous contents of elements, numerous reference Lower Paleozoic rocks were analysed to identify rock from which element was released into the fluid phase on the Permian hotline. Such a pre-Permian rock is the Silurian lydite, with the source association of P-Ti-Si-U-CO_2 and Silurian rhyolite with K-Rb-Ba source association. According to zonality of Devonian stratabound sulfidic mineralization of the Smolník type, from the vent centre on the sea floor, the metabasalt samples with disseminated sulfides were separately normalized in the central and transitional zones. That sulfidic and zoned mineralization was a source of elements Fe-**Mn**-Cu-Pb-Zn-B-F-Sn-Mo-K-Li-Sb-S. In the metamorphic facies and during the anatectic melting in the amphibolite facies, the elements were released from those source rocks into Permian fluid phase (Figs. 11 and 12, Tab. 5).

The gradual development of skarns formation in the Čučma area is compared to other skarns and greisen that were formed and identified in epidote-amphibolite facies or in the related biotite zone, in the chlorite-apatite and stilpnomelane-chlorite zone in Gemeric unit respectively. Three samples of Čučma skarns were compared using normalization to reference granite and added to the MMH cycle (Fig. 13). The grey muscovite-biotite (Ms/Bt) porphyric anatectic granite G from the Hnilec locality is a reference rock for the Lower and Middle Permian mineralizations – according to normalized REE contents identical with the upper crust. In this case the porphyric anatectic granite G has indistinct negative Eu anomaly, indicating the plagioclase origin from anatectic melt not differentiated in hot line on which the granite was formed (Fig. 11). So the contents of elements in porphyric granite G represent the reference upper crust, which underwent anatectic melting without a magmatic differentiation. The samples of hydrothermal mineralization as well as andesite samples from the Permian MMH cycle were normalized and compared in isocones to this crust (Fig. 13). In the Čučma area the fluid phase from the upper crust source created Fe bearing part and metasomatic part with rhodochrosite – kutnahorite of skarn, where contents of Fe-Mn-Ca-Cu-Zn-Ni-S are anomalous and Na-K-Sn-B-W-As association are depleted in comparison to reference porphyric granite G (Fig. 13; Radvanec & Gonda, 2019).

The reference rock for the second group of samples with the primitive mantle influence is represented by the fine-grained aplitic granite G2 from the Hnilec locality (Fig. 11). Contents of normalized REE in this granite, identical with primitive mantle, show a distinct negative Eu anomaly, related to the origin of plagioclase – albite from differentiated anatectic magma. The element contents in this fine-grained aplitic granite G2 represent a rock which underwent magmatic differentiation. Analyses of skarns and greisens of amphibolite facies, chlorite-apatite and stilpnomelane-chlorite zones with the primitive mantle nature and Permian rhyolite analyses were compared to this granite G2 in isocones (Fig. 14). The Mn skarn with spinels, Mn/Ti olivines, rhodonite and amphiboles from Čučma locality has positive Eu anomaly and according to primitive mantle influence, the isocone shows Mn-Mo-Cu-Zn-Co-Ba-V anomalies in comparison to reference aplitic granite G2. That Mn skarn of amphibolite facies is depleted of K-Rb-Li-Nb-Sn-W-Sb-Cs elements (Figs. 11 and 14). The source rock for the formation of Fe bearing part and metasomatic Mn bearing part with rhodochrosite-kutnahorite are the mentioned central and transitional Fe and Mn-rich zones of former fluid outflow from the vent centre on the sea floor. The see floor metabasalt with these disseminated sulfides was recognized in Devonian stratiform sulfide mineralization of Smolník type. The source of Ba, which is bound by baryte is from Silurian rhyolite in the Čučma skarn. Mineral associations and chemical composition of analysed samples of stratiform sulfidic mineralization confirm that the Silurian and Devonian mineralization is a main source of elements to Permian MMH cycle (Figs. 11 and 12).

Studying gradual formation of Fe and Mn skarns in the chlorite-apatite zone, then in the amphibolite facies and finally in the stilpnomelane-chlorite zone on the locality Čučma, closes the type variations of Mn-, Mg- and Fe-metasomatic/metamorphic and skarns mineralization in the former Silurian limestones. In the greenschists facies these limestones were usually replaced to the ankerite and siderite on several localities, like the siderite deposit Manó near Nižná Slaná. On the locality Dlhá dolina that former limestone was replaced to the dolomite, magnesite and to Fe skarn in the stilpnomelane-chlorite zone respectively (Grecula et al., 1995; Radvanec et al., 2010; Radvanec & Gonda, 2019). However most of the Silurian limestone layers were not metasomatically transformed and layers are still presents as marbles or metalimestones bodies in different occurrences from greenschists to amphibolite facies in Gemeric unit (Grecula et al., 2009).

Conclusions

Two lenticular ore bodies of Mn bearing skarn, closing a segment of Fe skarn, are located near the Čučma village, about 6 km north-east of Rožňava town in the Gemeric unit of the Internal (Inner) Western Carpathians. Skarns were formed in three successive stages. The first stage metasomatically replaced the former Silurian limestones lenses into of Mn-rich calcite, kutnahorite, rhodochrosite,

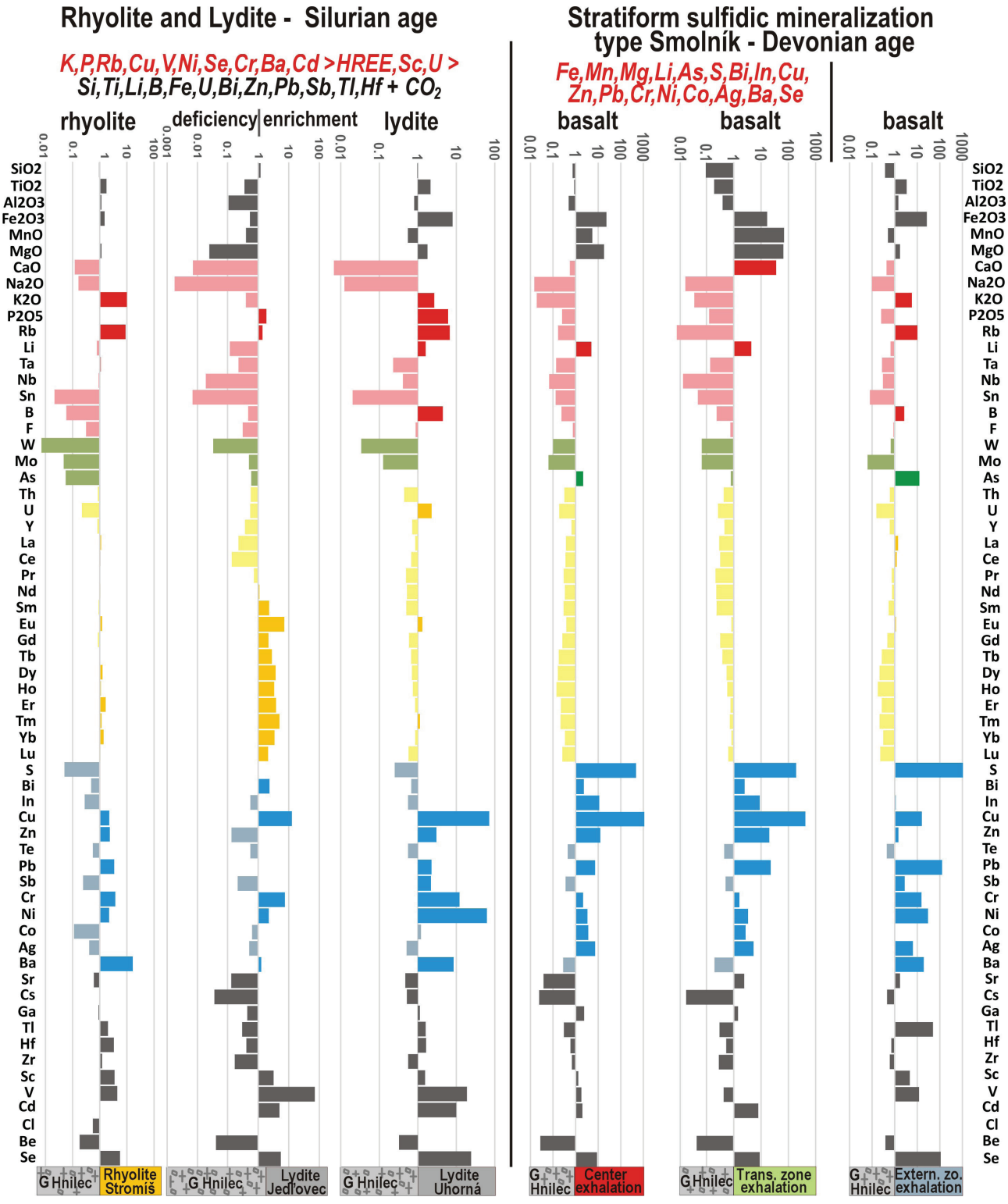

Fig. 12. The enrichment, depletion or isoconcentratiom – isocon of elements contents after their normalization in rhyolite (Tab. 5), lydites and samples of zonal stratabound sulfidic mineralization of the Smolník type was reported by Radvanec & Gonda (2019). According to sample classification by REE contents normalization to upper crust, the normalization logarithmically visualized the relation with the reference grey Ms/Bt porphyric granite G from the Hnilec locality. This normalization to granite G shows, which elements from rhyolite, lydites and stratabound mineralization were mobilized to metamorphic-magmatic-hydrothermal cycle in Permian.

Tab. 5
Bulk composition of rocks.

Rock	Fe skarn	Mn skarn	Mn Skarn	Rhyolite	Granite	Granite
Locality	Čučma	Čučma	Čučma	Stromiš	Súľová	Dlhá dolina
Assemblage	Mgh	Mn Cabonates	Ol.Man.Spinel. Pyl	Kfs	Ms-Bt	Ms
Stage/Metamor.	1	1	2 and 3	Greenschist	Amphibolite	Amphibolite
SiO_2 %	17.50	25.50	1.58	70.80	75.40	74.60
TiO_2	0.06	0.13	< 0.01	0.37	0.03	0.02
Al_2O_3	1.77	4.48	0.10	15.20	13.40	15.00
Fe_2O_3	55.60	3.18	0.87	1.58	1.17	0.62
MnO	8.98	43.80	85.70	0.02	0.07	0.03
MgO	1.75	0.67	0.08	0.28	0.03	0.27
CaO	6.33	7.90	0.44	0.08	0.19	0.94
Na_2O	0.13	0.03	0.04	1.00	3.65	5.16
K_2O	0.08	0.02	0.01	10.50	4.13	1.48
P_2O_5	0.32	0.11	< 0.01	0.08	0.20	0.58
S	0.39	0.18	0.08	< 0.02	< 0.02	< 0.02
Cl	< 0.01	< 0.01	< 0.01	< 0.01	< 0.01	< 0.01
F	0.07	0.07	< 0.05	< 0.05	0.26	1.12
LOI	7.41	13.2	9.87	0.65	0.93	0.87
SO_3 %	0.05	0.35	< 0.02	< 0.02	< 0.02	< 0.02
Rb mg/kg	4.1	1.3	0.3	161	739	488
Li	3.9	6.8	0.4	13.2	387	180
Ta	0.4	0.4	< 0.01	1.2	4.9	14.6
Nb	3.21	4.85	0.03	10.8	15.6	49.9
Sn	10	5	18	3	31	85
B	< 1	< 1	9	1	223	39
W	3	9	< 2	< 2	13	53
Mo	5	6	14	< 3	< 3	< 3
As	4	259	293	6	2	33
Th	2.3	3.1	< 0.5	15.2	8.6	8.7
U	0.8	2.2	< 0.5	2	4.8	21
Y	7.87	8.92	2.78	28.6	5.19	6.89
La	7.6	9.3	1.1	42	3	< 1
Ce	23.7	22.7	4.1	92.8	9.7	3.6
Pr	2.34	2.51	0.3	10.9	1.17	0.47
Nd	9.47	11.1	1.3	40.5	4.25	1.57
Sm	2.03	2.31	0.28	7.84	1.5	0.89
Eu	0.45	0.55	0.36	1.13	0.02	0.02

Tab. 5
Continuation

Rock	Fe skarn	Mn skarn	Mn Skarn	Rhyolite	Granite	Granite
Locality	**Čučma**	**Čučma**	**Čučma**	**Stromiš**	**Súľová**	**Dlhá dolina**
Assemblage	**Mgh**	**Mn Cabonates**	**Ol.Man.Spinel. Pyl**	**Kfs**	**Ms-Bt**	**Ms**
Stage/Metamor.	**1**	**1**	**2 and 3**	**Greenschist**	**Amphibolite**	**Amphibolite**
Gd	1.63	1.74	0.26	6.54	0.93	0.57
Tb	0.35	0.37	0.07	1.12	0.24	0.25
Dy	1.94	2.17	0.39	5.81	1.2	1.35
Ho	0.37	0.39	0.09	0.94	0.16	0.18
Er	1.17	1.22	0.29	3.04	0.42	0.5
Tm	0.15	0.17	0.04	0.33	0.06	0.09
Yb	0.98	1.05	0.25	2.25	0.4	0.68
Lu	0.15	0.15	0.04	0.37	0.05	0.08
Bi	< 5	< 5	< 5	< 5	< 5	8
In	< 0.05	< 0.05	0.07	< 0.05	0.13	0.12
Cu	147	24	58	9	10	6
Zn	290	156	479	44	66	38
Te	< 1	< 1	< 1	< 1	< 1	< 1
Pb	81	39	< 5	32	22	10
Sb	7.7	13.1	< 0.5	3.4	1.3	1.1
Cr	14	15	3	21	8	11
Ni	58	99	154	< 4	< 4	< 4
Co	37.9	196	175	1.1	0.5	0.4
Ag	< 0.4	< 0.4	< 0.4	< 0.4	< 0.4	< 0.4
Ba	261	44	1586	1013	11	24
Sr	120	163	53	32	3	33
Cs	11.5	0.9	< 5	8.2	53.8	22.2
Ga	13	10.4	10.1	14.2	21.9	32.3
Tl	0.1	< 0.1	< 0.1	1	3.4	1.3
Hf	5.8	11.9	16	5.7	3	3
Zr	30	23	1	164	48	28
Sc	2.6	2.6	0.2	13.4	3.2	8.4
V	85	38	24	42	< 1	< 1
Cd	0.5	0.2	0.5	0.1	0.1	0.1
Be	2.6	1.7	0.3	1.4	11.7	1.6
Se	< 1	< 1	< 1	< 1	< 1	< 1
Ge mg/kg	10	20	14	2	4	10

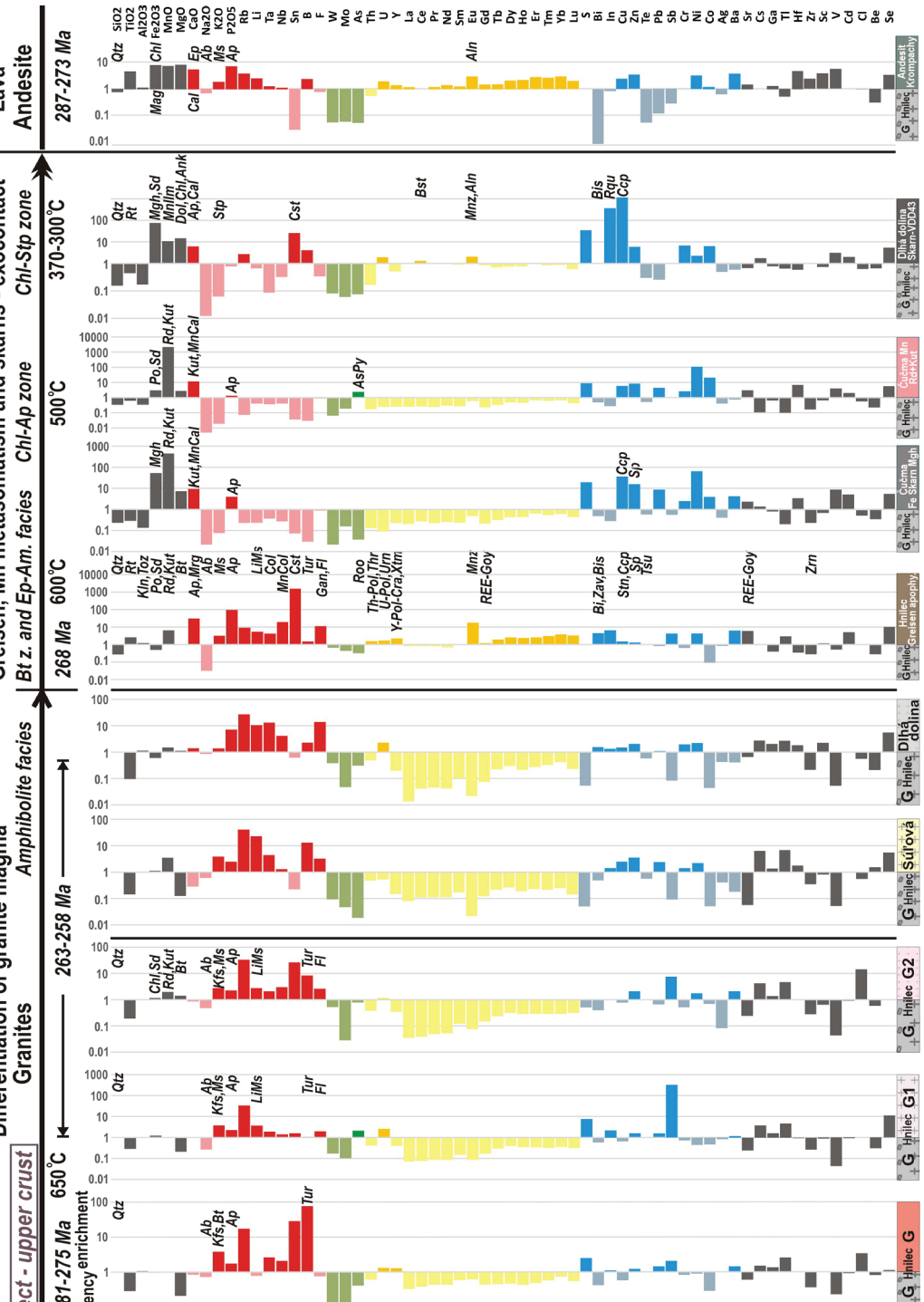

Fig. 13. Enrichment, depletion or isoconcentration – isocone of the elements contents are expressed by the ratio in logarithmic scale after normalization of elements contents of those in grey Ms/Bt porphyric granite G, representing melting of upper crust in the Hnilec locality. The principle of isocone values is explained in the text. According to samples classification, which are the same after the REE contents normalized to upper crust, the isocones were calculated in the greisen from the Hnilec apophysis, Fe-bearing skarn and rhodonite-kutnahorite rich metasomatic part of Čučma locality, in the skarn of borehole V-DD-43 in Dlhá dolina. These type mineralizations are located in epidote-amphibole facies, in biotite zone, in chlorite-apatite zone and in chlorite-stilpnomelane zone, being reported by Radvanec and Gonda (2019) and in Table 5. Isocones were calculated in normalization to grey Ms/Bt porphyric granite G, to Bt/Kfs porphyric granite G with pink phenocrysts of feldspar, and also to medium-grained Ms granite G1, fine-grained aplitic granite G2 of Hnilec locality, to medium-grained Ms-Bt granite of Súľová, in medium-fine grained Ms granite of Dlhá dolina and andesite. According this normalization there was found that Permian granites of S-type have increasing contents of K, P, Rb, Li, Ta, Nb, but mainly Sn, B and Sb. Andesite is depleted by association Sn, W, Mo, As, Bi and Te, characterizing greisens. Anomalous ratios in isocone are marked by the abbreviation of mineral – the main bearer of anomalous element. Abbreviations are explained in mineralogical figures.

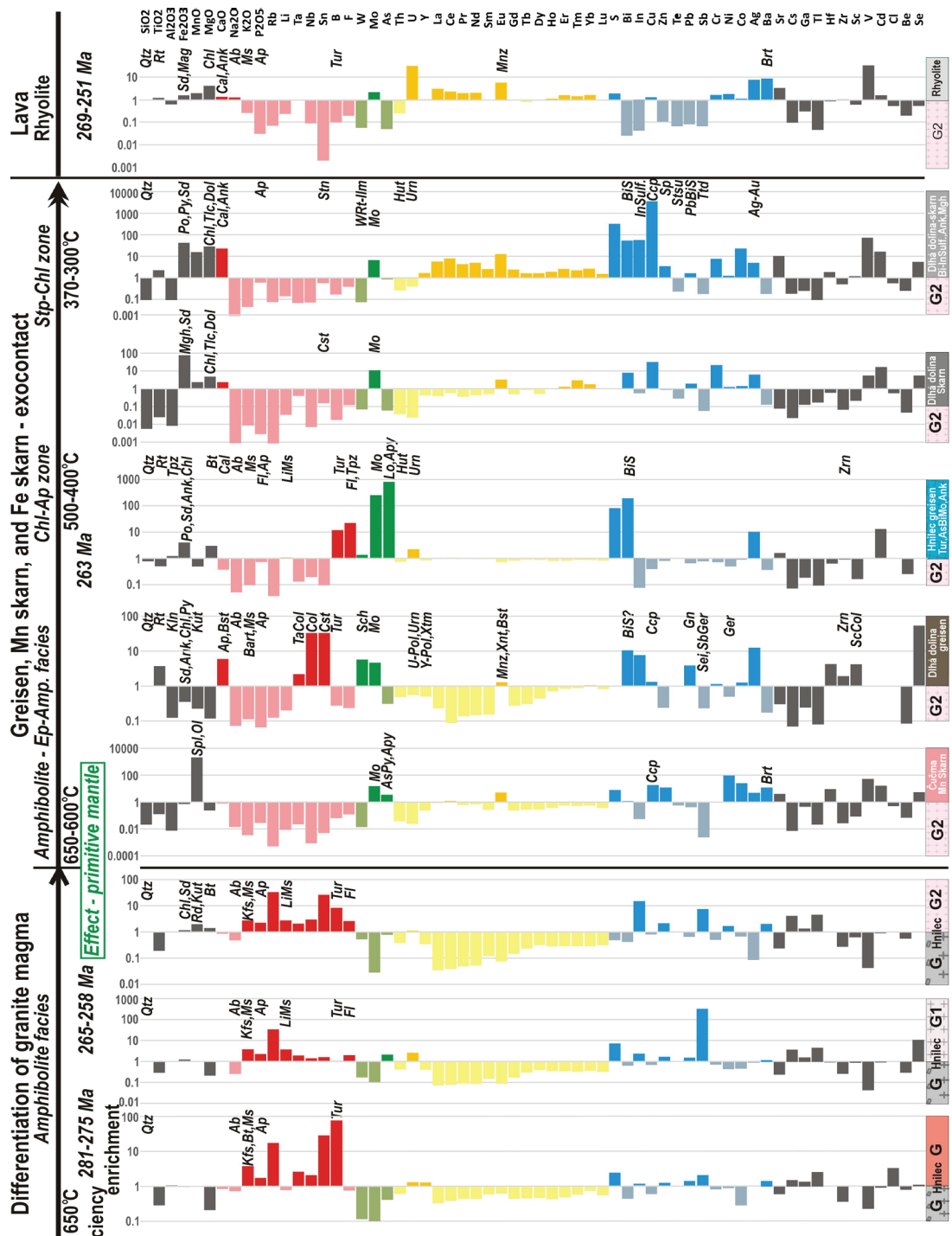

Fig. 14. Enrichment and deficiency of the elements content expressed by the ratio of normalized elements in logarithmic scale to elements in fine-grained aplitic granite G2, representing the differentiation of Permian granite melt with REE characteristic of primitive mantle. According to classification of samples, corresponding after normalization of REE contents to primitive mantle, the isocones were calculated in the Mn bearing skarn in Čučma, where metamorphic overprint with Ti-rich tephroite, Mn-olivines, spinels, rhodonite, manganosite and amphiboles was found, next in the Dlhá dolina greisen, the greisen with molybdenite and ankerite from Hnilec, in the skarn from the borehole VSV 05-2 in Elisabeth gallery – talc and magnesite deposit in Dlhá dolina and in the skarn of sulfidic zone in borehole V-DD-43 from the Dlhá dolina reported by Radvanec and Gonda (2019). These etalon mineralizations are located in amphibolite facies, chlorite-apatite and stilpnomelane-chlorite zones and reported by l.c. and in Table 5. Anomalous ratios in isocone are marked by abbreviation of mineral – the main bearer of anomalous element. Abbreviations are explained in mineralogical figures.

Mn-rich siderite, fluorapatite, tourmaline, phengitic muscovite, Mn-rich chlorite. The pyrite, molybdenite, galena, chalcopyrite, pyrite, sphalerite and Ag-rich tetrahedrite there occur as well. Near a contact of former limestone with metapelite, the maghemite dominates over assemblage of Mn-rich carbonates to form Fe skarn. The metasomatic first stage formed in the chlorite-apatite zone at a temperature range 520–540 °C where formation of maghemite and Mn-rich carbonates was controlled by the fluid phase, released during anatectic melting of the upper crust during the older Permian metamorphic-magmatic-hydrothermal cycle (MMH of 281–273 Ma).

In the second prograde metamorphic stage, the first-stage minerals were continuously overheated in amphibolite facies at 600–650 °C, forming minerals as follow: spessartine, alleghanyite, pyrophanite, manganosite, kempite, jacobsite, iwakiite, hausmannite, tephroite, Ti-rich tephroite, knebelite, rhodonite-1, rhodonite-2, cummingtonite, grunerite and allanite. Grains formation of Ti-rich tephroite are controlled by the sector zoning and the individual sectors were quantified by TiO_2 content. In the sector with the lowest content, TiO_2 ranges from 0.14 to 0.32 wt.%, in the next sector the range is from 1.44 to 2.96 and the sector with a maximum TiO_2 content ranges from 4.83 to 6.22. In the chemical formula of the sectors, the Ti content ranges from 0.008 to 0.159 (apfu) and Si from 0.842 to 0.981 respectively. It shows that the Ti content substituted Si up to 0.159 apfu, having different content of Ti in each sectors and an immiscibility gap between the individual sectors are determined by a new $Ti^{4+} = Si^{4+}$ substitution in the olivine group.

In the third and final stage of skarns formation, the unstable minerals of previous two stages were replaced by the Si, Ba, H_2S and H_2O bearing fluid phase to form Ca-rich spessartine, bementite, pyrochroite, quartz, pyrolusite, baryte, chlorite and stilpnomelane during the retrograde stilpnomelane-chlorite zone, ranging from 300 to 370 °C. The prograde (second) and retrograde (third) metamorphic stages produced a part of Mn skarn that has the positive Eu anomaly and was formed by the fluid phase influenced by the primitive mantle in younger MMH cycle of the Permian, according by dating in the period of 269–251 Ma.

Three successive formations of skarns describe 39 empiric reactions and the source of Fe, Mn and Ba necessary to skarns formation was released to fluid phase by anatectic melting of the Silurian rhyolite and Devonian stratabound sulfidic mineralization in the Permian amphibolite facies metamorphism.

Acknowledgement

Authors express their thanks to Ministry of Environment of Slovak Republic for funding the metallogenetic research, based on the project *Raw material potential of Slovak Republic – analysis and prognostic re-evaluation of critical raw materials*. The remarks and suggestions of one anonymous reviewer and Z. Németh are greatly appreciated.

References

Akimoto, S. & Syono, Y., 1972: High pressure transformations in $MnSiO_3$. *Amer. Mineralogist, 57, 76–84.*

Bartalský, J., Grecula, P., Bárta, R., Rozložník, L., Snopko, L., Varček, C., Varga, J., Ilavský, J. & Ťapák, M., 1973: Geologicko-ložisková štúdia Spišsko-gemerského rudohoria. *Spišská Nová Ves, Geol. Priesk.*

Beardi, J. S. & Tracy, R. J., 2002: Spinels and other oxides in Mn-rich rocks from the Hutter Mine, Pittsylvania County, Virginia, U.S.A.: Implications for miscibility and solvus relations among jacobsite, galaxite, and magnetite. *Amer. Mineralogist, 87, 690–698*.

Brown, P., Essene, E. & Peacor, D., 1980: Phase relations inferred from field data for Mn pyroxenes and pyroxenoids. *Contr. Mineral. Petrol., 74, 417–425.*

De Capitani, C. & Peters, T., 1981: The solvus in the system $CaCO_3$– $MnCO_3$. *Contr. Mineral. Petrology, 76, 394–400.*

Chang, L. L. Y., Howie R. A. & Zussman, J., 1998: Non-Silicates: Sulphates, Carbonates, Phosphates, Halides (Rock-Forming Minerals), 2nd Ed., Vol. 5b.

Faryad, S. W., 1994: Mineralogy of Mn-rich rocks from greenschist facies sequences of the Gemericum, West Carpathians, Slovakia. *Neu. Jb. Mineral., Mh., 10, 464–480*.

Fonarev, V. I., Korolkov, G. Ya. & Dokina, T. N., 1977: Experimental study of the assemblage cummingtonite + magnetite + quartz, $P_T = P_{H2O}$ = 1000kg/cm^2, NNO buffer. *Contr. Physiochem. Petrol. (Nauka, Mocsow), VI, 224–235.*

Gilbert, M. C., Helz, R. T., Popp, R. K. & Spear, F. S., 1982: Experimental studies of amphiboles stability. *Rev. Miner., 9b, Miner. Soc. Amer., 229–267.*

Grecula, P., Abonyi, A., Abonyiová, M., Antaš, J., Bartalský, B., Bartalský, J., Dianiška, I., Ďuďa, R., Gargulák, M., Gazdačko, Ľ., Hudáček, J., Kobulský, J., Lörincz,, L., Macko, J., Návesňák, D., Németh, Z., Novotný, L., Radvanec, M., Rojkovič, I., Rozložník, L., Varček C. & Zlocha, J., 1995: Mineral deposits of the Slovak Ore Mountains. Vol. 1. *Bratislava, Geocomplex, 1–834.*

Grecula, P. (ed.), Kobulský, J., Gazdačko, Ľ., Németh, Z., Hraško, Ľ., Novotný, L. & Maglay, J., 2009: Geologická mapa Spišsko-gemerského rudohoria 1 : 50 000. *Bratislava, Ministerstvo život. prostr. Slovenskej republiky – Št. Geol. Úst. D. Štúra.*

Ito, J., 1972: Rhodonite-pyroxmangite peritectic along the join MnSiO – MgSiO in air. *Amer. Mineralogist, 57, 865–876.*

Kantor, J., 1953: Mangánové ložisko pri Čučme. *MS. Bratislava, archive SGIDŠ, 1–32.*

Kantor, J., 1954: Origin of manganese ore in Spišsko-gemerské rudohorie Mts. *Geol. Práce, Zpr., 1, 70–71 (in Slovak)*.

Kohút, M. & Stein, H., 2005: Re-Os molybdenite dating of granite-related Sn-W-Mo mineralization at Hnilec, Gemeric Superunit, Slovakia. *Mineral. Petrol., 85, 117–129.*

Kohút, M., Trubač, J., Novotný, L., Ackerman, L., Demko, R., Bartalský, B. & Erban, V., 2013: Geology and Re-Os molybdenite geochronology of the Kurišková U-Mo deposit (Western Carpathians, Slovakia). *J. Geosci., 58, 271–282.*

Peterec, D. & Ďuďa, R., 2003: Zriedkavé minerály Mn-ložiska pri Čučme. *Natura Carpatica, 44, 229–236*.

Peterec, D. & Ďuďa, R., 2009: Mangánová mineralizácia na lokalite Čučma. *Minerál, 17, 410–414*.

Momoi, H., 1964. Mineralogical study of rhodonites in Japan, with special reference to contact metamorphism. *Mem. Fac. Sci., Kyushu Univ., ser. D – geol., 15, 39–63.*

Radvanec, M., Grecula, P. & Žák, K., 2004: Siderite mineralization of the Gemericum superunit (Western Carpathians, Slovakia): review and revised genetic model. *Ore. Geol. Rev., 24, 3–4, 267–298.*

Radvanec, M., Konečný, P., Németh, Z. & Grecula, P., 2007: P-T-t dráha a lokálne anatektické tavenie metapelitu s prímesou psamitického kremeňa vo variskej metamorfóze gemerika. *Miner. Slov., 39, 1–44.*

Radvanec, M., Németh, Z. & Bajtoš, P. (eds.), Koděra, P., Prochaska, W., Roda, Š., Tréger, M., Baláž, P., Grecula, P., Cicmanová, S., Kráľ, J. & Žák, K., 2010: Magnesite and talc in Slovakia – Genetic and geoenvironmental models. *Bratislava, Št. Geol. Úst. D. Štúra, 1–189.*

Radvanec, M., Konečný, P., Ondrejka, M., Putiš, M., Uher, P. & Németh, Z., 2009: Granity gemerika ako indikátor extenzie kôry nad neskorovariskou subdukčnou zónou a pri ranoalpínskej riftogenéze (Západné Karpaty): interpretácia podľa veku monazitu a zirkónu datovaného metódou CHIME a SHRIMP. *Miner. Slov., 41, 381–394*.

Radvanec, M. & Grecula, P., 2016: Geotectonic and metallogenetic evolution of Gemericum (Inner Western Carpathians) from Ordovician to Jurassic. *Miner. Slov., 48, 104–118.*

Radvanec, M., Németh, Z., Kráľ, J. & Pramuka, S., 2017: Variscan dismembered metaophiolite suite fragments of Paleo-Tethys in Gemeric unit, Western Carpathians. *Miner. Slov., 49, 1–48.*

Radvanec, M. & Németh, Z., 2018: Variscan epidote-eclogite, blueschists and pumpellyite actinolite facies Cpx/Sr-rich epidote-metagabbro blocks exhumed in Carboniferous, with Permian amphibolite facies overprint (Gemeric unit, Western Carpathians). *Miner. Slov., 50, 55–99.*

Radvanec, M. & Gonda, S., 2019: Genetic model of Permian hydrothermal mineralization in Gemeric unit (W. Carpathians) from the deep-seated zone of anatectic melting to volcanic-exhalative SedEx mineralization on the surface. *Miner. Slov., 52, 109–156.*

Rojkovič, I., 1999: Manganese mineralization in the Western Carpathians, Slovakia. *Geol. Carpath., 50, 191–192*.

Rojkovič, I., 2001: Early Paleozoic manganese ores in the Gemericum Superunit Western Carpathians, Slovakia. *Geolines, 13, 34–41*.

Ružička, P., Bačík , P., Myšľan, P. & Kurylo, S., 2020: Grossular and diopside in crystalline limestone from the locality Čučma-Čierna baňa (Slovak Republic). *Bull. Mineral. Petrol., 28, 1, 94–104, ISSN 2570-7337*.

Sun, S. S. & McDonough, W. F., 1989: Chemical and isotopic systematics of oceanic basalts; implications for mantle composition and processes. In: Saunders, A. D. & Norry, M. J. (eds.): Magmatism in the ocean basins. *London, Geol. Soc. London, 42, 313–345.*

Števko, M., Plecháček, J., Venclík, V. & Malíková, R., 2015: Hausmannite and manganosite from the Čučma – Čierna baňa manganese deposit (Slovak Republic). *Bull. mineral.-petrol. Odd. Nár. Muz. (Praha), 23, 1.*

Vozárová, A. & Vozár, J., 1988: Late Paleozoic in West Carpathians. *Bratislava, Geol. Úst. D. Štúra, 1–314.*

Vozárová, A., Presnyakov, S., Šarinová, K. & Šmelko, M., 2015: First evidence for Permian-Triassic boundary volcanism in the Northern Gemericum: geochemistry and U-Pb zircon geochronology. *Geol. Carpath., 66, 5, 375–391.*

Postupný vznik Fe a Mn skarnov na lokalite Čučma v gemeriku: od metasomatózy s následnou rekryštalizáciou v amfibolitovej fácii a vznikom Ti tefroitu až po retrográdnu metamorfózu v stilpnomelánovo-chloritovej zóne

Neďaleko obce Čučma asi 6 km severovýchodne od Rožňavy (Vnútorné Západné Karpaty; obr. 1) sa v gemeriku vyskytujú dve šošovkovité telesá Mn skarnu uzatvárajúce segment Fe skarnu. Skarny sa formovali v troch po sebe nasledujúcich etapách. V prvom štádiu sa metasomaticky zmenili šošovky pôvodných silúrskych vápencov z holeckých vrstiev (Grecula et al., 2009) na Mn kalcit, kutnahorit, rodochrozit, Mn siderit, fluoroapatit, turmalín, fengitický muskovit a Mn chlorit. V tomto Mn metasomatite sa zistil aj pyrit, molybdenit, galenit, chalkopyrit, pyrit, sfalerit a Ag tetraedrit. Blízko kontaktu pôvodného vápenca s metapelitom dominuje maghemit nad Mn uhličitanmi (obr. 3). Táto poloha Fe skarnu má čiernu farbu, je slabo magnetická a je prevažne jemne zrnitá (obr. 2). Metasomatóza pôvodného vápenca vznikla v chloritovo-apatitovej zóne v teplotnom rozsahu 520 – 540 °C (Mn-karbonátový termometer; De Capitani a Peters, 1981; Chang et al., 1998), kde z fluidnej fázy uvoľnenej počas anatektického tavenia vrchnej kôry vznikol maghemit a Mn uhličitany (obr. 11). Táto metasomatóza vznikla v staršom permskom metamorfnom magmaticko-hydrotermálnom cykle (MMH) v datovanom období 281 – 273 mil. r. (Radvanec a Gonda, 2019).

V druhom štádiu sa minerály prvého metasomatického štádia kontinuálne metamorfovali v amfibolitovej fácii pri 600 – 650 °C a tlaku nižšom ako 4 kbar (geotermo-

barometre; Ito, 1972; Broun et al., 1980; Akimoto a Syono, 1972; Fonarev et al., 1977; Gilbert et al., 1982). V tomto štádiu vznikla skupina Mn granátov, humity, oxidy, halogenidy, spinely, olivíny, pyroxenoidy a amfiboly. Tieto skupiny minerálov tvoria mladšiu časť Mn skarnu s nasledujúcou asociáciou: spessartín, alleghanyit, pyrofanit, manganozit, kempit, jakobsit, iwakiit, hausmannit, tefroit, Ti tefroit, knebelit, rodonit-1, rodonit-2, kummingtonit, grunerit a allanit (obr. 2 až 7).

Jednotlivé zrná Ti tefroitu sú zložené zo sektorov a jednotlivé sektory sú kvantifikované obsahom TiO_2 v hmot. % (obr. 7, tab. 4). V sektore s najnižším obsahom je obsah TiO_2 od 0,14 do 0,32 hmot. %. V ďalšom sektore je rozpätie od 1,44 do 2,96 a v sektore s maximálnym obsahom TiO_2 je jeho rozsah v rozmedzí 4,83 až 6,22 hmot. %. V chemickom vzorci sektorov je obsah Ti v rozsahu od 0,008 do 0,159 (apfu) a obsah Si od 0,842 do 0,981. V každom sektore je obsah Ti substituovaný obsahom Si postupne až do hodnoty 0,159 apfu a medzi jednotlivými sektormi sa zistila aj medzera nemiešateľnosti. Substitúciu Ti a Si medzi sektormi Ti tefroitu určuje substitúcia $Ti^{4+} = Si^{4+}$, ktorá je v skupine olivínu novozistená, rovnako ako aj Ti tefroit (obr. 8).

V tretej, poslednej fáze tvorby skarnov boli nestabilné minerály z predchádzajúcich dvoch štádií zmenené v retrográdnej metamorfóze stilpnomelánovo-chloritovej zóny v rozmedzí od 300 do 370 °C, pričom retrográdnu metamorfózu kontrolovala fluidná fáza s obsahom Si, Ba, H_2S a H_2O. V tomto treťom štádiu vývoja Mn skarnu vznikol Ca spessartín, bementit, pyrochroit, kremeň, pyroluzit, baryt, chlorit a stilpnomelán (obr. 2 až 7).

Prográdna (druhé štádium) a retrográdna (tretie štádium) metamorfóza postupne vytvorila časť Mn skarnu, ktorý má pozitívnu anomáliu Eu. Vznik tejto časti Mn skarnu bol ovplyvnený primitívnym plášťom a vznikol v mladšom MMH cykle v období permu od 269 do 251 mil. r. (Radvanec a Gonda, 2019, obr. 11).

Tri po sebe nasledujúce štádiá vzniku Fe a Mn skarnov opisuje 39 empirických reakcií. Zdroj Fe, Mn a Ba potrebný na tvorbu hlavných minerálov a barytu v Fe a Mn skarne sa uvoľnil do fluidnej fázy počas anatektického tavenia silúrskeho ryolitu a z devónskej stratiformnej sulfidickej mineralizácie počas permskej metamorfózy v amfibolitovej fácii (obr. 10 až 14).

Doručené / Received: 17. 7. 2020
Prijaté na publikovanie / Accepted: 18. 2. 2021